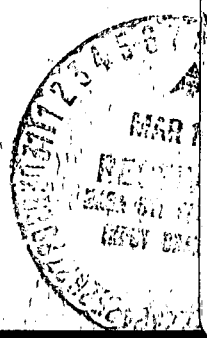

CALIFORNIA INSTITUTE OF TECHNOLOGY

MAGNETOSPHERIC ACCESS OF SOLAR PARTICLES AND THE CONFIGURATION OF THE DISTANT GEOMAGNETIC FIELD

Thesis by

Lawrence Curtis Evans

Volume Two

APPENDIX A

Additional Observations

This appendix provides a summary of all proton events observed with OGO-4 and observed flux profiles for several events which can be referred to in the context of the discussion in Section VII. Due to the time-sharing nature of the OGO-4 telemetry, it is not possible to obtain a single profile which illustrates all of the features necessary for Section VII. Table A-1 tabulates all of the proton events observed with OGO-4 and indicates pertinent data relating to the orientation of the interplanetary magnetic field. Most of the data in this table are also depicted in figure V-5.

The events whose profiles are presented here are divided into three classes: EDP events (normally associated with co-rotating features), solar flare events, and events having characteristics of both EDP events and flare events (class C events). A description of these classes of events and the criteria used to distinguish between EDP events and flare events are discussed in Sections V and VI. In addition, the 1 December 1967 EDP event and the 2 November 1967 solar flare event are discussed in some detail in Section V. Accompanying the profiles of each event here is a brief list of the more notable observational features of the event. Events are presented chronologically to facilitate finding any specific one.

All presentations of profiles in this thesis conform to the following conventions (the assignment of the terms α-pole and β-pole is

Table A-1

OGO-4 -- Observed Persistent Polar Cap Features: 1-40 MeV Protons

First Observation Date	Univ. Time (HHMM)	Total Elpsd. Time (hrs.)	$\max\left(\frac{LPL}{HPL}\right)$	Pole Sector % Southern Solar Field	Event Phase R=Rise D=Decay E=EDP	Obsrvd?	Enhancements $\max\left(\frac{HPL}{LPL}\right)$	Enhancements Durations (hrs.)
30 Jul 67	1820*	>13.2	12.5	N - 58%	D	N		
1 Aug 67	1745	> 5.7†	4.0	N - 0%	R	N		
	2140	> 1.8†	1.3	S - 0%	R	N		
11 Aug 67	0155*	> 8.2	1.7	N - 33%	E	Y	1.3	3.5
12 Aug 67	1620*	> 5.7	1.4	N - 100%	R	N		
19 Aug 67	0320*	>10.4†	6.8	N - 44%	E	Y	1.7	>2.0†
	0410*	> 3.1	3.4	S - 44%	E	N		
24 Aug 67	1345	> 5.8†	37.0	N - 75%	R	N		
19 Sep 67	0305*	>29.2†	6.6	N - 47%	R D	N		
9 Oct 67	0040	> 1.2†	3.0	N - 100%	R	N		
27 Oct 67	1730*	> 6.8	2.8	S + 15%	D	N		
1 Nov 67	1540	14.7	4.0	N - 97%	R D	N		
2 Nov 67	1115*	>24.4†	7.2	N - 90%	R D	N		
	1150*	> 3.2†	3.9	S - 100%	R	N		
	3305*	> 1.9	1.0	S - 100%	R	Y	2.3	>1.9
4 Nov 67	2200	8.8	2.2	S + 66%	D	N		
10 Nov 67	2025	3.2	2.3	S + 100%	E	N		
	2110	> 3.3†	2.7	N + 100%	E	Y	1.3	>1.4†
14 Nov 67	0330*	>42.5†	1.7	N - 37%	R	Y	1.1	>1.6†
	1210	> 1.6†	0.9	S - 50%	R	N		
18 Nov 67	0200*	>11.5	1.3	N - 87%	D	Y	1.3	1.6
24 Nov 67	1730	> 6.5†	3.2	N - 69%	R	N		

Table A-1 (continued)

First Observation Date	Univ. Time (HHMM)	Total Elpsd. Time (hrs.)	max(LPL/HPL)	Pole Sector	% Southern Solar Field	Event Phase R=Rise D=Decay E=EDP	Enhancements Obsrvd?	max(HPL/LPL)	Durations (hrs.)
27 Nov 67	0900	14.7	6.3	N +	46%	R			
	0950	>38.0†	15.9	S +	73%	R D	N		
1 Dec 67	1800*	>13.0	5.6	S +	82%	E	Y	1.5	1.4
	1850	> 4.7†	1.3	N +	100%	E	Y	2.2	>3.7†
2 Dec 67	0700	11.5	2.1	S +	46%	E	Y	1.4	>1.0†
	0935	> 4.7†	1.9	N +	43%	E	Y	1.9	>1.0†
5 Dec 67	0015	>13.8	1.2	N -	27%	D	Y	1.3	4.9
17 Dec 67	0105*	>24.5	6.6	N -	--	RE	N		
	0825	5.0	0.8	S -	--	E	Y	1.7	5.0
18 Dec 67	1610	>16.2†	2.0	N -	--	R	N		
	0715	>13.2†	1.6	S -	--	RE	Y	1.8	8.1
30 Dec 67	1045	6.8	4.5	S +	0%	E	Y	3.5	>1.0
	1130	6.5	6.2	N +	0%	E	Y	1.9	1.6
10 Jan 68	2150*	>10.5†	1.8	N -	60%	D	N		
1 Feb 68	2010	11.4	1.2	N -	26%	R D	Y	1.1	3.3
8 Feb 68	1805*	>31.0†	25.2	N -	100%	D	N		
9 Feb 68	1515*	>11.2†	15.8	N -	100%	R D	N		
12 Feb 68	0640	3.2	1.4	N -	38%	R	N		
13 Feb 68	1335	> 3.2†	2.1	N +	53%	R	N		
	0930*	> 6.6†	1.8	S +	24%	R	N		
14 Feb 68	0630*	> 8.3†	1.3	S +	0%	D	Y	1.4	>1.6†
15 Feb 68	1015	>13.8†	2.0	S +	--	R D	N		
26 Feb 68	1120	5.7	15.8	S +	0%	R	N		
	1210	1.6	17.8	N +	0%	R	N		
	1700	8.0	1.6	N -	62%	D	Y	1.6	7.4
	2415	1.5	1.6	S -	100%	E?	Y	1.6	1.5

Table A-1 (continued)

First Observation Date	Univ. Time (HHMM)	Total Elpsd. Time (hrs.)	$\max\left(\frac{LPL}{HPL}\right)$	Pole Sector	% Southern Solar Field	Event Phase R=Rise D=Decay E=EDP	Obsrvd?	Enhancements $\max\left(\frac{HPL}{LPL}\right)$	Enhancements Duration (hrs.)
9 Mar 68	2305*	>24.4†	4.8	N -	45%	R D	N		
21 Mar 68	2330	>13.2†	2.5	S +	43%	R D	N		
15 Apr 68	0010*	> 3.4	0.9	S +	--	D	Y	1.5	>3.4
24 Apr 68	0730*	>40.5†	5.0	N -	67%	R D	N		
	2115	> 6.6	3.2	S -	46%	R	N		
26 Apr 68	1930*	> 6.5	21.0	N -	85%	D	N		
27 Apr 68	1330	34.2	2.2	N -	36%	R D	N		
	2400	5.0	1.5	S -	50%	R	N		
29 Apr 68	1725	> 3.2†	1.6	N -	9%	R	N		
5 May 68	2200*	> 4.8†	1.4	S +	38%	D	N		
13 May 68	2130*	>45.5†	≃1.0	S +	--	D	Y	1.6	>45.5†
10 Jun 68	1720*	>29.2	1.4	N -	63%	D	N		
9 Jul 68	0415	4.8	1.4	N +	67%	R	N		
	1210	1.9	2.0	N +	0%	R	N		
	1000*	>11.3†	2.5	S +	18%	R D	N		
13 Jul 68	0215*	> 4.8	1.6	N -	--	D	N		
13 Jul 68	1025	>38.9†	>4.2	N -	20%	R D	Y	1.2	>27.6†
14 Aug 68	1645	> 6.5†	4.0	S +	85%	R	N		
21 Aug 68	1315	> 8.2†	4.0	N -	100%	E	N		
	1545	1.5	2.5	S -	100%	E	N		
28 Sep 68	0220	> 6.5†	1.4	N -	39%	D	N		
	1120	> 8.2†	1.6	S +	56%	R	N		
	1345*	> 3.2	1.5	N +	100%	R	N		
29 Sep 68	0415	> 3.5†	1.1	N +	100%	R	N		
	0500	>14.8†	1.8	S +	64%	R D	N		

Table A-1 (continued)

First Observation Date	Univ. Time (HHMM)	Total Elpsd. Time (hrs.)	$\max\left(\frac{LPL}{HPL}\right)$	Pole Sector	% Southern Solar Field	Event Phase R=Rise D=Decay E=EDP	Enhancements Obsrvd?	Enhancements $\max\left(\frac{HPL}{LPL}\right)$	Enhancements Duration (hrs.)
29 Sep 68	2345	8.0	1.8	N -	25%	R D	N		
	2745	> 3.2	1.5	S -	31%	D	N		
30 Sep 68	1420*	> 8.1†	1.8	N -	72%	R D	N		
4 Oct 68	0400	>37.5†	2.2	N -	32%	R D	N		
	0815	> 9.8	1.6	S -	51%	R	N		
	3410	3.3	1.5	S -	62%	D	N		
4 Nov 68	2340*	> 1.6†	1.8	S +	0%	D	N		
18 Nov 68	2330*	>24.2	2.5	N -	--	D	N		
	2600*	> 3.2†	1.5	S -	100%	D	N		

*Observation of the beginning of the event was prevented by the unavailability of the pertinent data.

†Persistent feature was observed in the last appropriate polar pass prior to a period during which the pertinent data were unavailable.

reproduced from table VII-1 in table A-2):

1. The horizontal axis is always time, expressed in terms of hours of universal time. Tick marks are placed every hour, and are labelled every six hours, consistent with clarity.
2. The vertical axis is always observed flux of 1.2-40 MeV protons ($V_1\overline{V_3}$) expressed in units of $(cm^2\text{-sec-sr})^{-1}$.
3. Error bars are indicated for representative points for flux levels below 10 $(cm^2\text{-sec-sr})^{-1}$, and all other points of comparable flux can be assumed to have comparable precision. If no error bars are indicated, they may be assumed to be smaller than the size of the dot used to indicate the observation, which is the case for all flux levels greater than 10 $(cm^2\text{-sec-sr})^{-1}$.
4. The region in which a profile was observed is indicated by the type of line connecting the data points:

   solid line --- low polar latitudes (LPL)

   dashed line --- α-pole high polar latitudes (α-HPL)

   dotted line --- β-pole high polar latitudes (β-HPL)
5. Separate observations of α-HPL fluxes are not indicated unless significantly different than the flux at LPL.
6. Interplanetary sector structure (positive, negative, or uncertain) is indicated at each sector reversal or change (indicated by long vertical lines). If no sector changes occur during the period covered by the profiles, the predominant sector for the period is stated in the legend.
7. The roles of α-pole and β-pole are assumed to change coincident

TABLE A-2

Correspondence Between α-pole/β-pole
North/South Geomagnetic Poles

	North Pole	South Pole
Positive Interplanetary Sector	α-pole	β-pole
Negative Interplanetary Sector	β-pole	α-pole

with a sector reversal. If a period of uncertain sector is encountered, the previous assignment of α-pole and β-pole rôles is maintained until the sector becomes definable.

8. Missing data are indicated by arrows pointing downward near the top of the figure. The arrows are labelled to indicate the pole for which data are missing due to a gap in the available data (*G*), or due to a pass which does not reach a sufficiently high invariant latitude to penetrate the high polar latitude region (*L*). In the latter case, of course, only HPL data should be missing; LPL observations should not be affected. The occasional exception to this is the south polar pass which does not reach a high enough invariant latitude to be above the rigidity cutoff latitude at any time. Such missing data are labelled *V* (very low pass) to indicate that LPL data are also unavailable. If the data are available but are contaminated by telemetry noise, the label *N* is used.
9. Sudden commencements and sudden impulses are indicated in the same manner as on the OGO-4 Data Coverage Plots: sudden commencements are represented by a triangle, sudden impulses by a diamond. Confirmed observations are represented by solid symbols, unconfirmed by open symbols.

Table A-3 lists all symbols and abbreviations used on the profiles.

Table A-3a

Standard Symbols Used on Event Profiles

Symbol	Meaning
α	α-pole (See Table E-2)
β	β-pole (See Table E-2)
•———	Low polar latitude profile
•– – –•	α-pole high polar latitude profile
••••••	β-pole high polar latitude profile
+	Data not available
▲	Confirmed sudden commencement
Δ	Unconfirmed sudden commencement
♦	Confirmed sudden impulse
◊	Unconfirmed sudden impulse
I	Representative ±1σ error bars
+	Positive interplanetary magnetic field sector
-	Negative interplanetary magnetic field sector
0	Indeterminate interplanetary magnetic field sector

Table A-3b

Standard Abbreviations Used on Event Profiles

Abbreviation	Meaning
G	Data gap
HPL	High polar latitude
L	Low pass (HPL data unavailable)
LPL	Low polar latitude
N	Data degraded by noise
SR	Sector reversal in interplanetary magnetic field
UT	Universal time
V	Very low pass (HPL and LPL data unavailable)

Figure A-1

11 August 1967 -- Class C Event

1. Very high fluxes: statistical errors are much smaller than dots used to represent data points.

2. The extremely rapid decay is a strong indication that this is not a flare event. The sudden commencement at 0555 UT and the weak depression in the sea level neutron monitor [48] tend to confirm that this is an EDP event. The absence of a feature in the α-HPL profile is, however, inconsistent with normal appearance of an EDP event. In addition, the delay between the LPL peak and the β-HPL peak ($\sim$2.0 hours) is much smaller than that normally associated with EDP events ($\sim$6.6 hours).

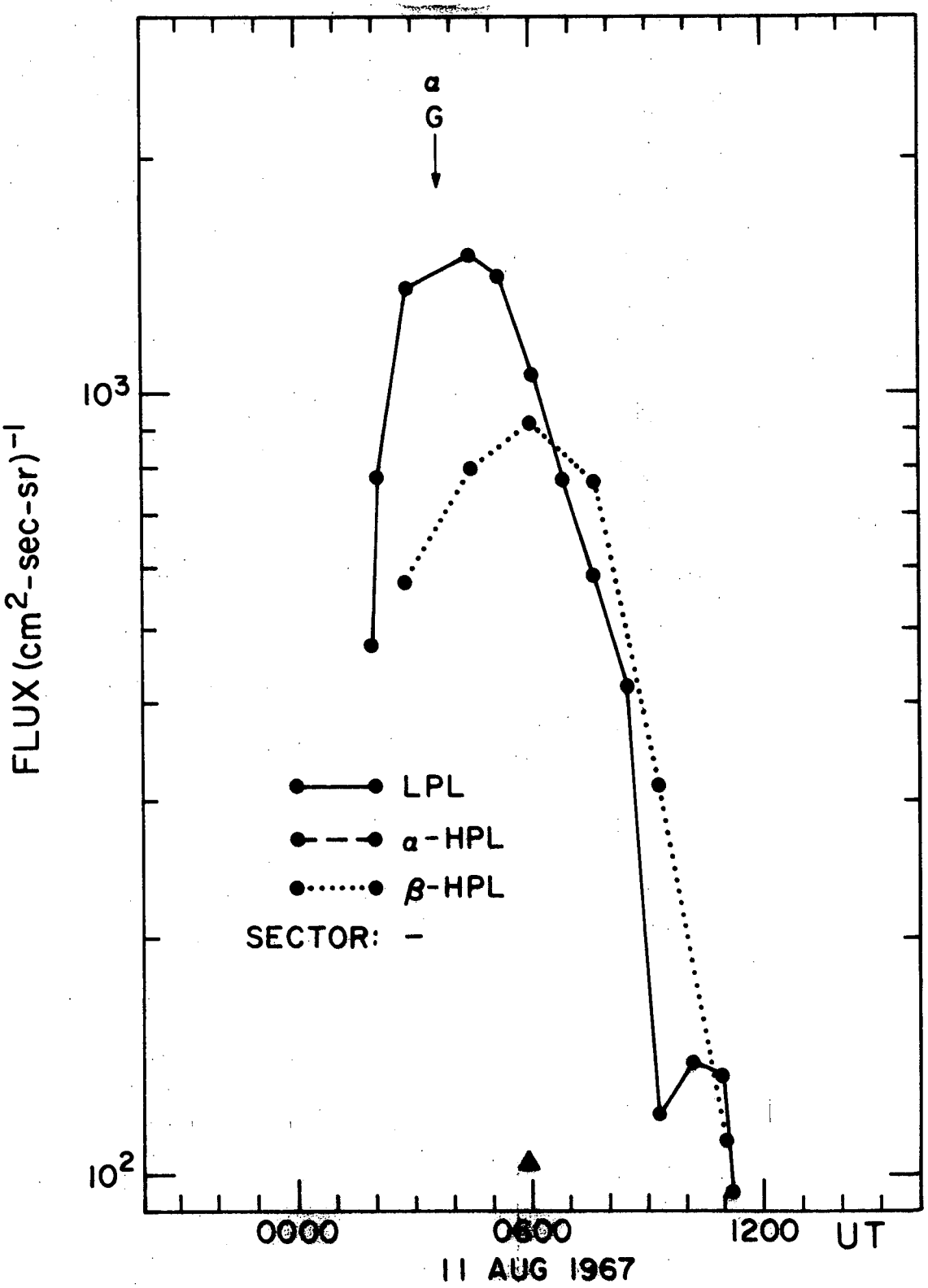
α
G
10^3
10^2
FLUX (cm^2-sec-sr)$^{-1}$
LPL
α-HPL
β-HPL
SECTOR: −
0000
0600
1200
UT
11 AUG 1967

Figure A-2

19 August 1967 -- EDP Event

1. This event is superimposed on the decay phase of an earlier flare event.

2. The LPL peak and α-HPL peak are clearly delineated.

3. The β-HPL flux continues to decay normally during the period of peak flux in the other two regions.

4. The data gap at $\sim$2200 UT prevents the observation of the complete β-HPL peak, although the beginning of this peak is observed at $\sim$1940 UT. Because of the low rates, the probability that this flux is a statistical variation from the LPL flux is $\lesssim 4.2 \times 10^{-8}$. Although this is not as statistically significant as most observations of features, and although there is only the one point, it is nonetheless consistent that the β-HPL flux at $\sim$1940 UT is part of the β-HPL EDP peak.

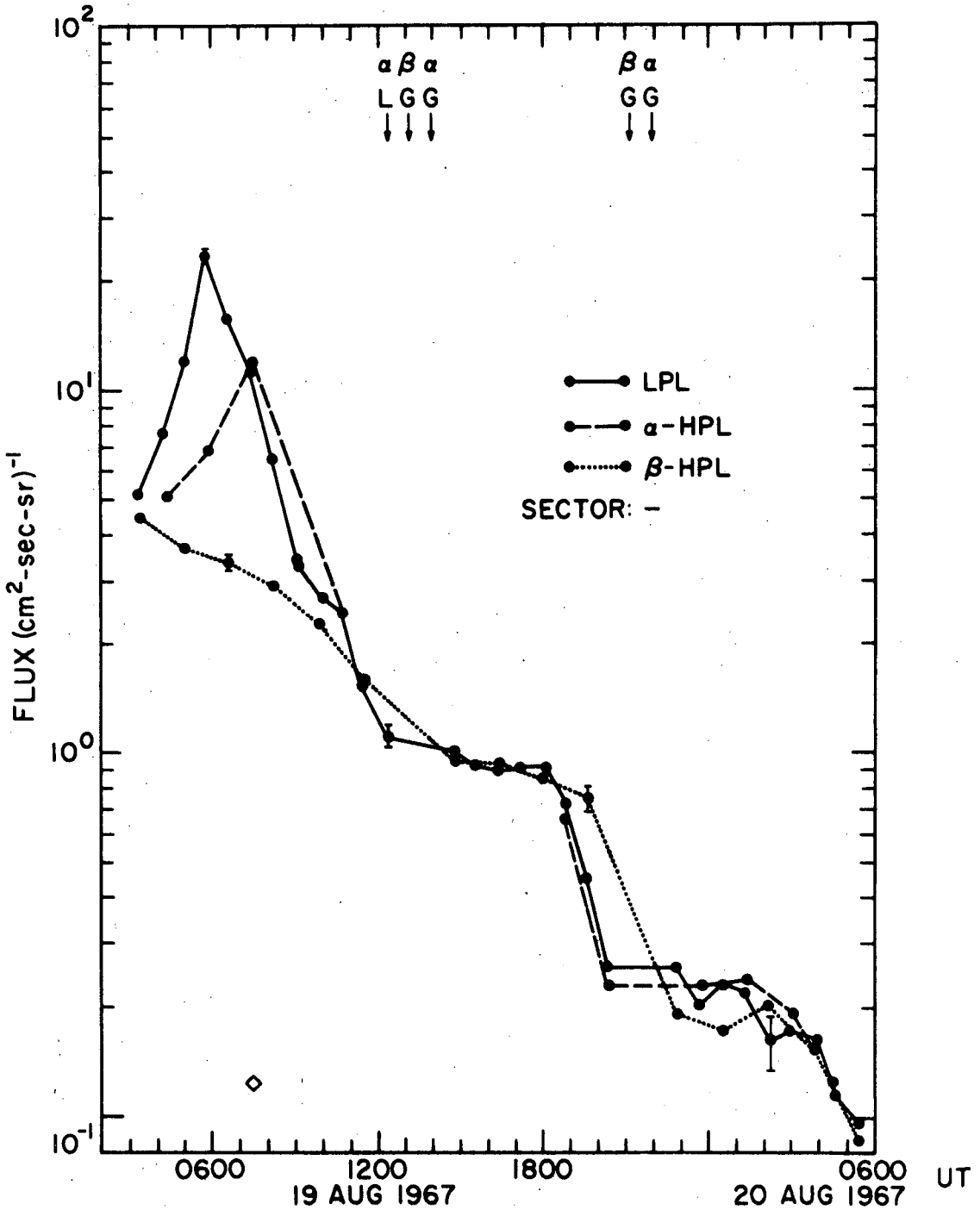
10^2
10^1
10^0
10^{-1}
FLUX (cm^2-sec-sr)$^{-1}$
α β α
L G G
β α
G G
LPL
α-HPL
β-HPL
SECTOR: –
0600
1200
1800
0600
UT
19 AUG 1967
20 AUG 1967

Figure A-3

2 November 1967 -- Flare Event (see also Section V)

1. This is an excellent example of a persistent feature. The feature in the β-pole is observed to last for the entire period from ∿1120 UT on 2 November to ∿1140 UT on 3 November (24+ hours). The data suggest that, but for the data gaps before and after this period, the feature might have been observed for a slightly longer period.

2. While the last north pole (β-pole) observation prior to the sector reversal at ∿1300 UT on 3 November contained the feature, the first north pole observation after this sector reversal did not show the feature.

3. A significant persistent feature is observed in the α-pole lasting for ∿3 hours starting with the observation at ∿1200 UT on 2 November.

4. The onset of the flare event is delayed in both HPL regions.

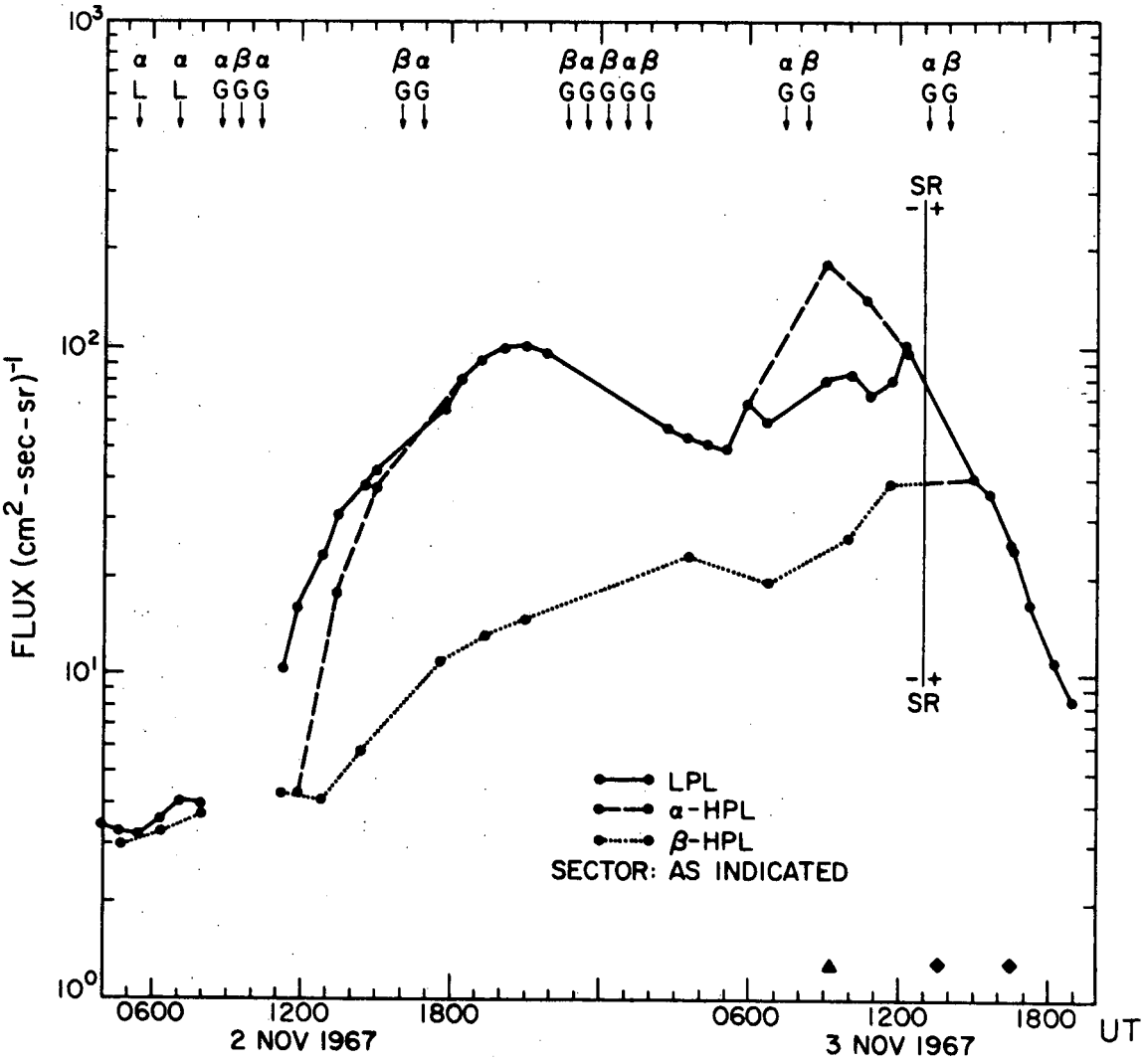
α α αβα βα βαβαβ αβ αβ
L L GGG GG GGGGG GG GG
SR
SR
LPL
α-HPL
β-HPL
SECTOR: AS INDICATED
FLUX (cm²-sec-sr)⁻¹
10³
10²
10¹
10⁰
0600
1200
1800
2 NOV 1967
0600
1200
1800
3 NOV 1967
UT

Figure A-4

10 November 1967 -- EDP Event

1. This EDP gives a good resolution of the LPL flux peak and the α-HPL flux peak. The appearance of a higher value for the α-HPL flux peak may be somewhat misleading: the actual maximum LPL flux may not have been observed due to the mechanics of the satellite orbit.

2. The β-HPL flux peak is not observed for this event. It should, of course, be noted that a sector reversal occurs before (∿0100 UT on 11 November) one might expect to observe a peak in this region (perhaps ∿0300 to ∿0600 UT on 11 November). Any conclusion drawn here should, however, be tempered somewhat by the degradation of the observations caused by the two data gaps following the sector reversal: 50% of the observations pertinent to this point are missing.

3. It is interesting that the flux in the post-sector reversal β-HPL region does not fluctuate in the same manner as that in the LPL region, but instead remains rather constant. This is consistent with a picture in which, immediately after a sector reversal, the access region associated with the new β-HPL region propagates with the solar wind, thus continuing to sample the same interplanetary flux, for the time necessary for the solar wind to carry the access region to a position consistent with the newly-established field

configuration (4-8 hours for a position 1000-2000 $R_\oplus$ behind the previous position). Again, this observation must be tempered by the precaution mentioned above.

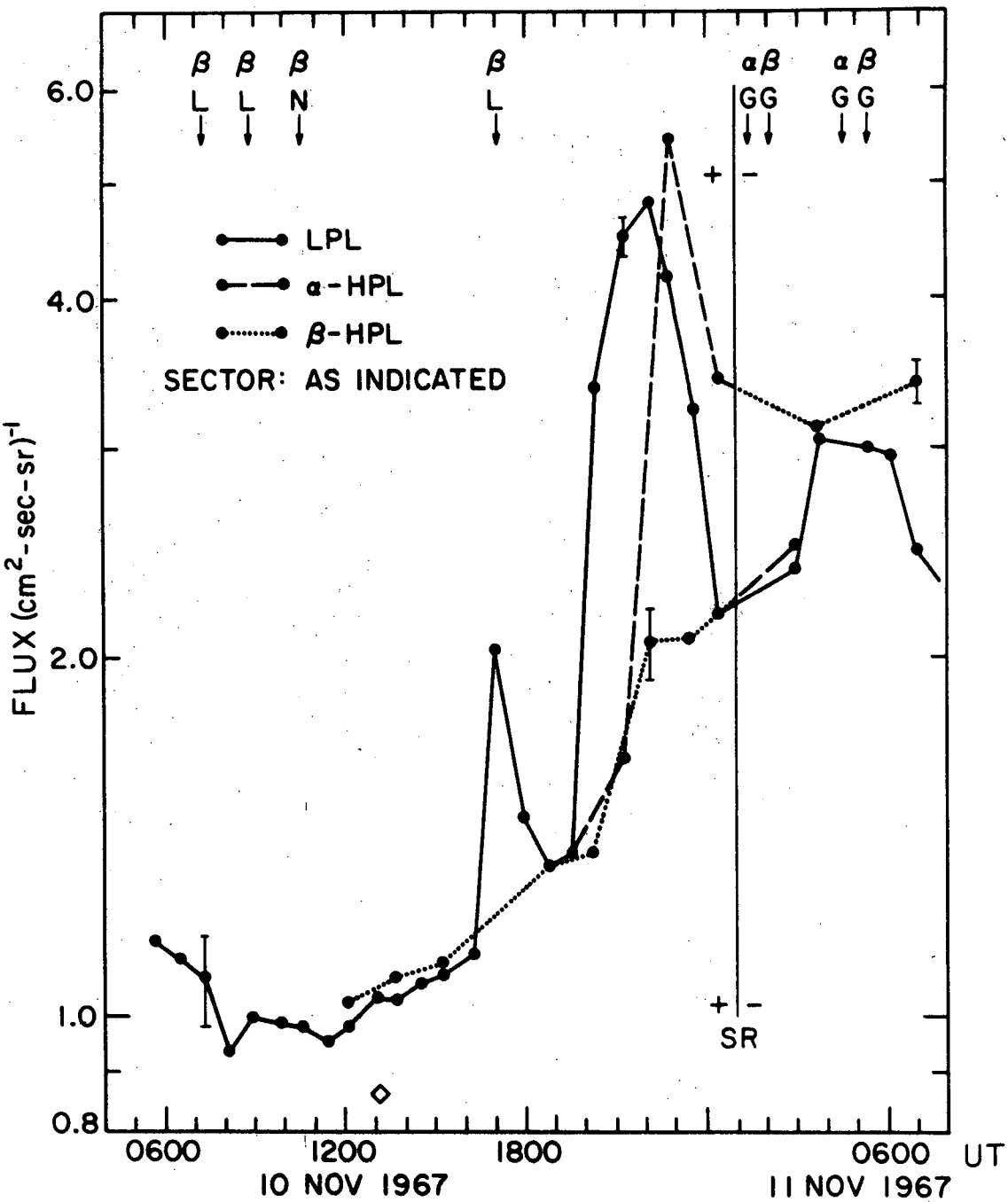
β β β β αβ αβ
L L N L GG GG
6.0
4.0
2.0
1.0
0.8
LPL
α-HPL
β-HPL
SECTOR: AS INDICATED
+ −
+ −
SR
FLUX (cm²-sec-sr)⁻¹
0600
1200
1800
0600
UT
10 NOV 1967
11 NOV 1967

Figure A-5

1 December 1967 -- EDP Event (see also Section V)

1. This profile is a definitive illustration of an EDP event being observed first on the LPL region, shortly thereafter in the α-HPL region, and finally, after a delay of ∿6½ hours, in the β-HPL region.

2. The flux observed in the β-HPL region gives every sign of being independent of variations in the fluxes observed in the other two regions. The reverse also appears to be true.

3. Indications of the independence of the fluxes in the LPL region and the α-HPL region with respect to each other are also clear.

4. The width of the α-HPL flux peak as presented in figure A-5 is misleading: an inherently poor time resolution (∿100 minutes between points) is compounded by the ubiquitous spectre of a data gap.

5. Poor time resolution may also be partly responsible for the much lower peak flux observed in the β-HPL region.

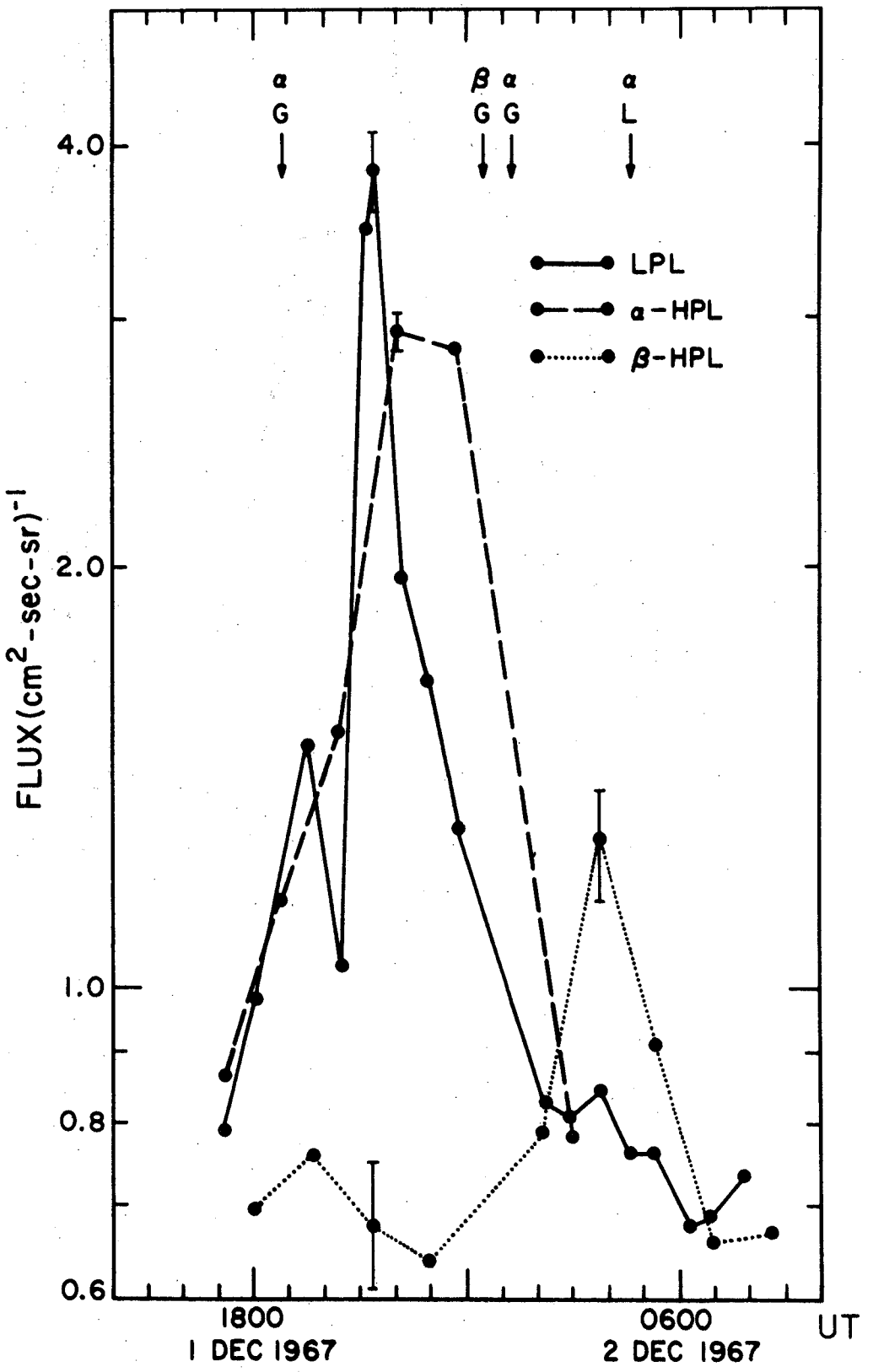
α G
β G
α G
α L
LPL
α-HPL
β-HPL
4.0
2.0
1.0
0.8
0.6
FLUX(cm²-sec-sr)⁻¹
1800
1 DEC 1967
0600
2 DEC 1967
UT

Figure A-6

2 December 1967 -- EDP Event

1. All of the expected three peaks (LPL, α-HPL, and β-HPL) are resolved and appear in the expected order. The observation of the precise temporal relationships among these flux peaks is seriously degraded, however, by the two data gaps at ∿1100-1200 UT and ∿1500-1600 UT. In spite of this expected degradation, at least the following two observations are clear:
    a. Both HPL flux peaks begin after the beginning of the LPL flux peak.
    b. The LPL flux peak ends before, or at least coincident with, both of the HPL flux peaks.

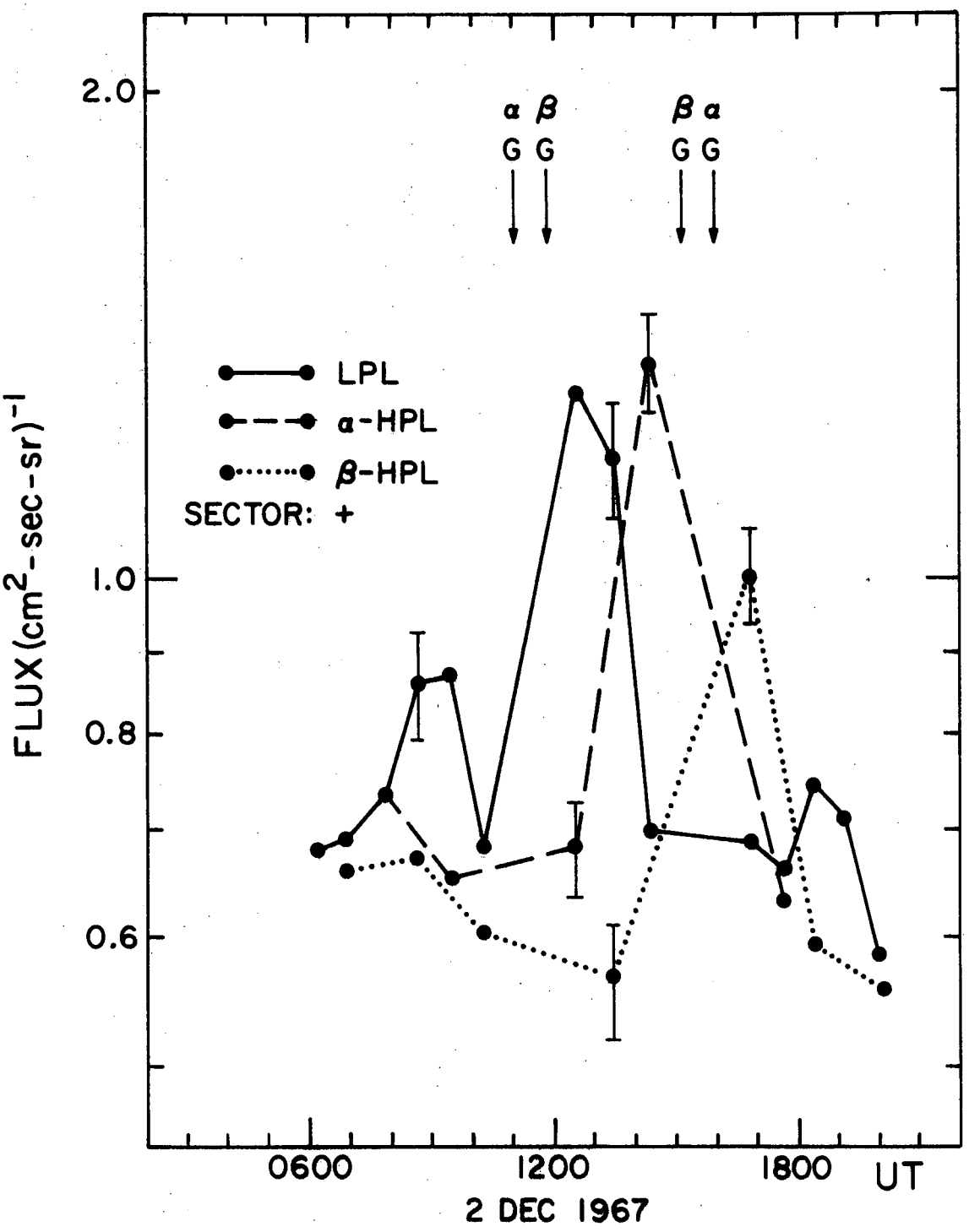
2.0
1.0
0.8
0.6
α β
G G
β α
G G
LPL
α-HPL
β-HPL
SECTOR: +
FLUX (cm²-sec-sr)⁻¹
0600
1200
1800
UT
2 DEC 1967

Figure A-7

30 December 1967 -- EDP Event

1. Profiles of LPL flux and α-HPL latitude flux both show a double-peaked structure.

2. The observation of the second β-HPL flux peak may have been prevented by the configuration of the satellite orbit: during the β-pole (south pole) passes at ∿2030 UT and ∿2210 UT, the satellite orbit did not reach a maximum invariant latitude large enough for penetration of the HPL region.

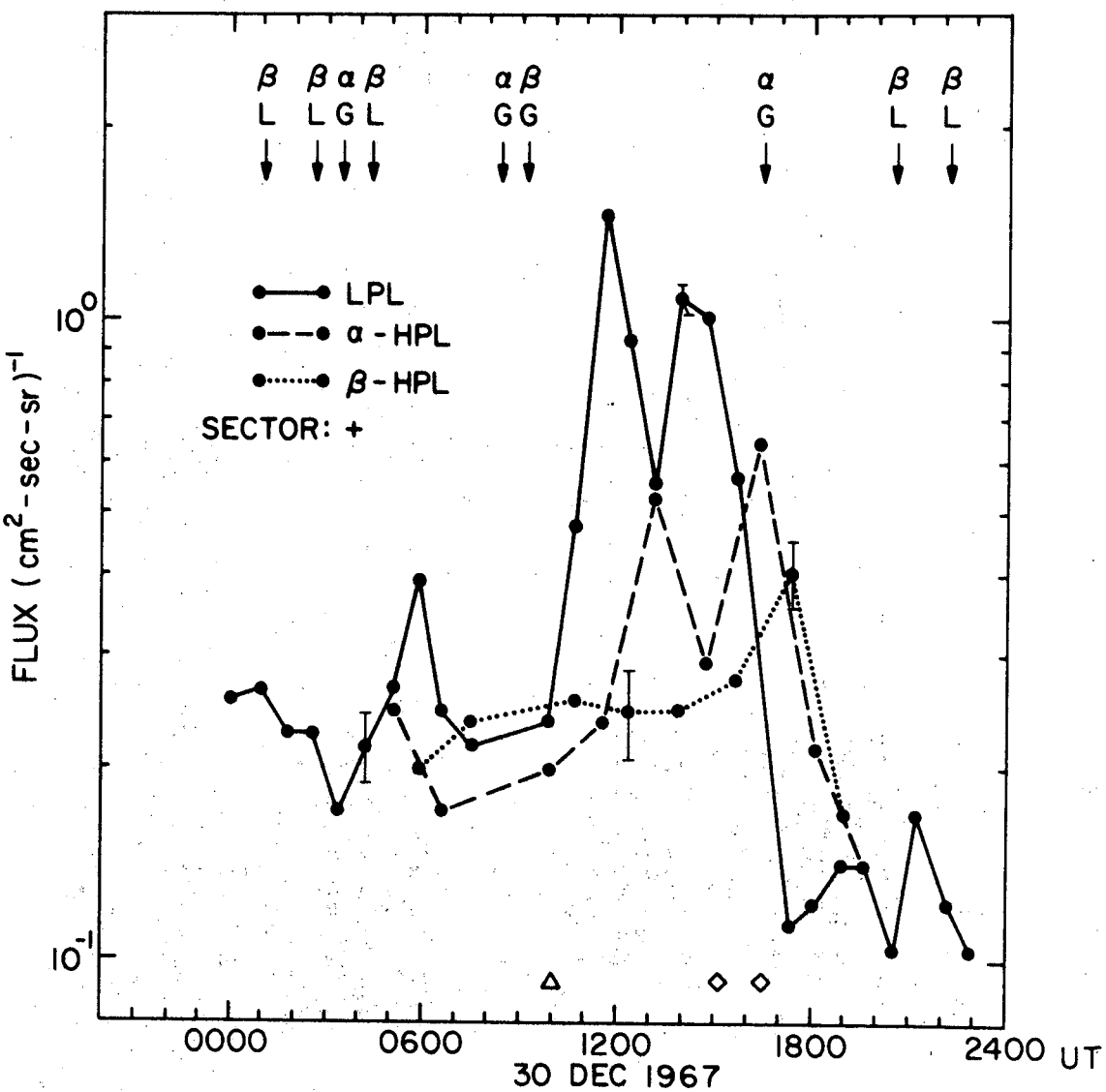
β L
β L
α G
β L
α G
α G
β L
β L
LPL
α - HPL
β - HPL
SECTOR: +
FLUX (cm²-sec-sr)⁻¹
10⁰
10⁻¹
0000
0600
1200
1800
2400 UT
30 DEC 1967

Figure A-8

1 February 1968 -- Solar Flare Event

1. This is a particularly good example of a flare event in which the β-HPL flux "crosses over" the LPL and α-HPL flux (at ∿0220 on 2 February). Unfortunately, the omnipresent data gap nearly destroys observations of the event. Nevertheless, there are indications that the β-HPL flux remained at a higher level than the LPL flux until the small LPL enhancement at ∿0640 on 2 February. This higher β-HPL flux is, of course, observed as an enhancement in the high latitude region of the β-pole.

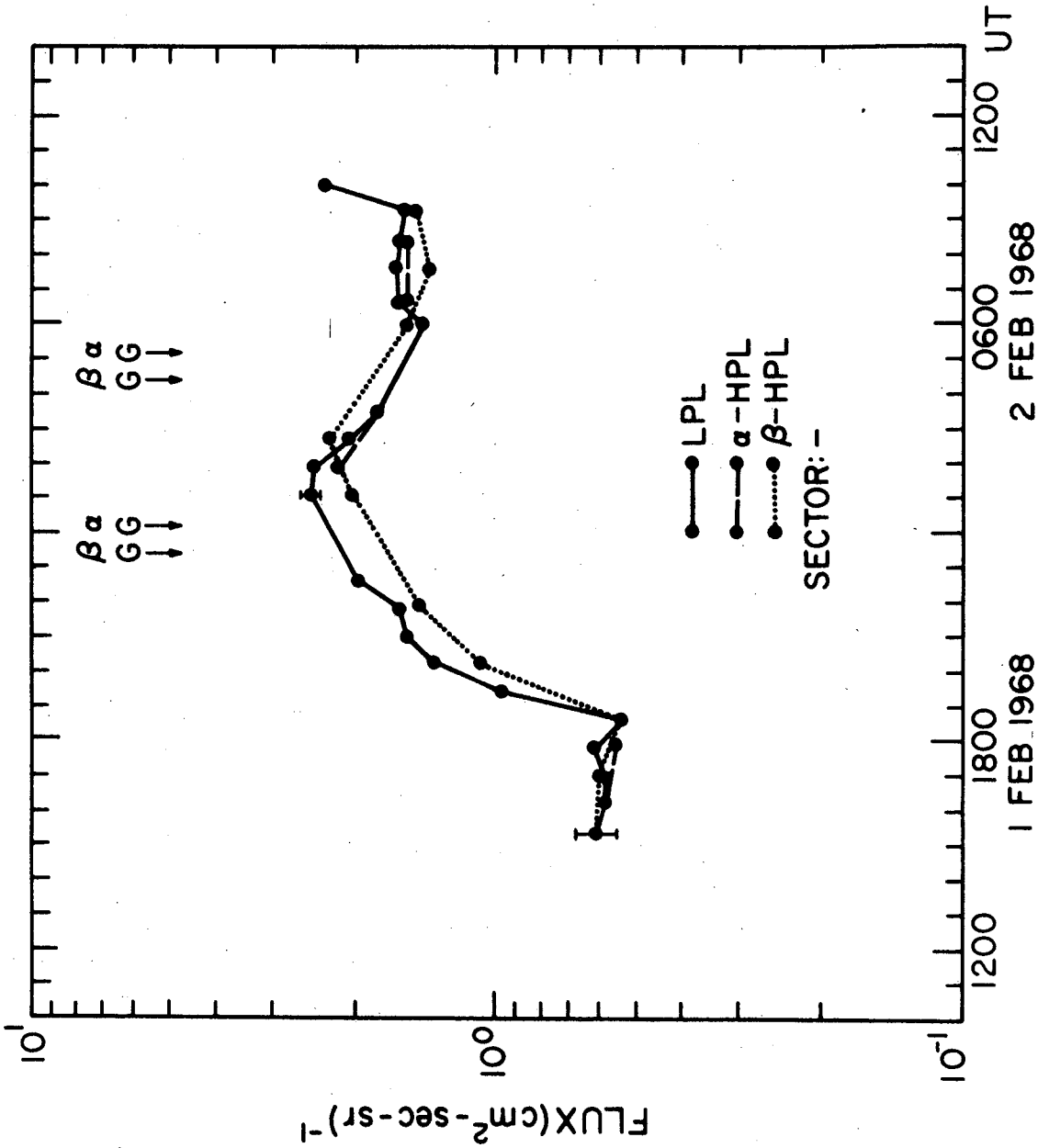
FLUX (cm^2-sec-sr)$^{-1}$
10^1
10^0
10^{-1}
1200
1800
1 FEB 1968
0600
2 FEB 1968
1200 UT
LPL
α-HPL
β-HPL
SECTOR: -
βα
GG
βα
GG

Figure A-9

8 February 1968 -- Solar Flare Event

1. This profile illustrates a long period observation of a persistent feature which is, with a few exceptions, quite large. The ratio of the LPL flux to β-HPL flux reaches a maximum in excess of 25:1. The feature persists from the beginning of the profile at ∿1720 UT on 8 February to ≳0100 UT on 10 February, a period of ≳31½ hours (see no. 2, below).

2. The duration of this persistent feature is interrupted by the period of uncertain sector structure from ∿0230 UT to ∿1400 UT on 9 February. During this "uncertain" period there would appear to be times (≲0530 UT and, perhaps, ∿1200 UT to ∿1400 UT on 9 February) when the β-HPL flux tends to approach the LPL flux more closely. Unfortunately, the behavior of the β-HPL flux *vis-á-vis* the LPL flux from ∿0230 UT to ∿0530 UT on 9 February is somewhat less definitive due to the data gap. The β-HPL peak at ∿1400 UT on 9 February is possibly a flux enhancement, considering the continuous appearance of the β-HPL decay from ∿0530 UT to ∿2330 UT on 9 February if the observations at ∿1200 UT and ∿1330 UT are omitted.

3. A sector reversal occurs at ∿0550 on 10 February, and, although it is significant that the first north polar observation after the

sector reversal shows no feature, the period of missing data immediately preceding the sector reversal (includes two β-HPL passes) somewhat clouds the question of the simultaneity of the feature disappearance and sector reversal.

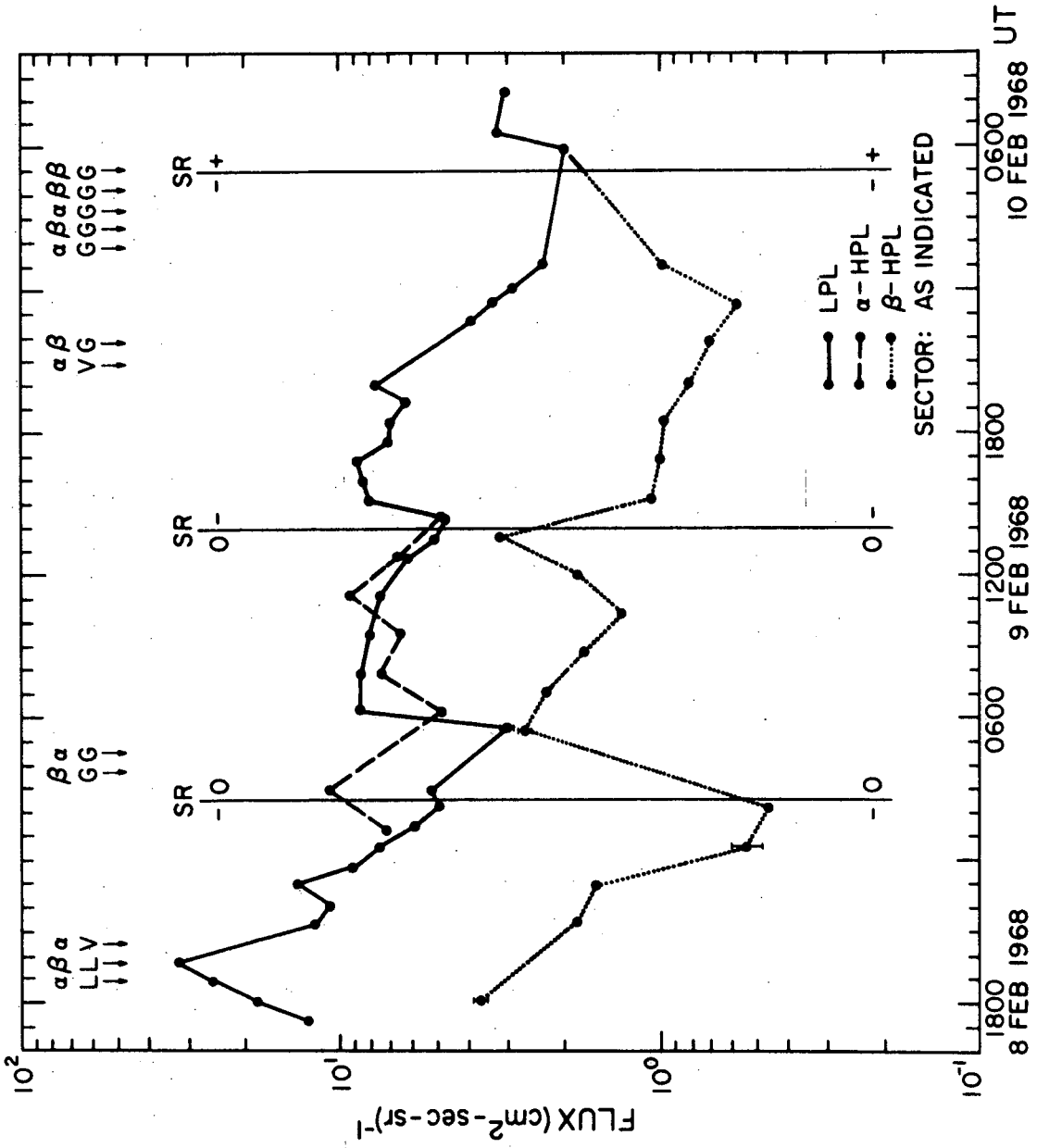
FLUX (cm²-sec-sr)⁻¹
10²
10¹
10⁰
10⁻¹
αβα LLV
βα GG
αβ VG
αβαββ GGGGG
SR
SR
SR
LPL
α-HPL
β-HPL
SECTOR: AS INDICATED
1800 8 FEB 1968
0600
1200 9 FEB 1968
1800
0600 10 FEB 1968 UT

Figure A-10

27 April 1968 -- Class C Event

1. A β-HPL feature (depression) is observed for a period of ∿34 hours during the rise and decay of this event.

2. A α-HPL depression is observed for ∿6½ hours beginning at ∿0000 on 28 April.

3. The flux increase observed at ∿0130 UT on 29 April at LPL is not observed at α-HPL until 0200-0340 UT, and not at β-HPL until later still.

4. The beginning of another persistent β-HPL feature is observed at ∿1600 UT on 29 April, but no data are available past ∿2200 UT.

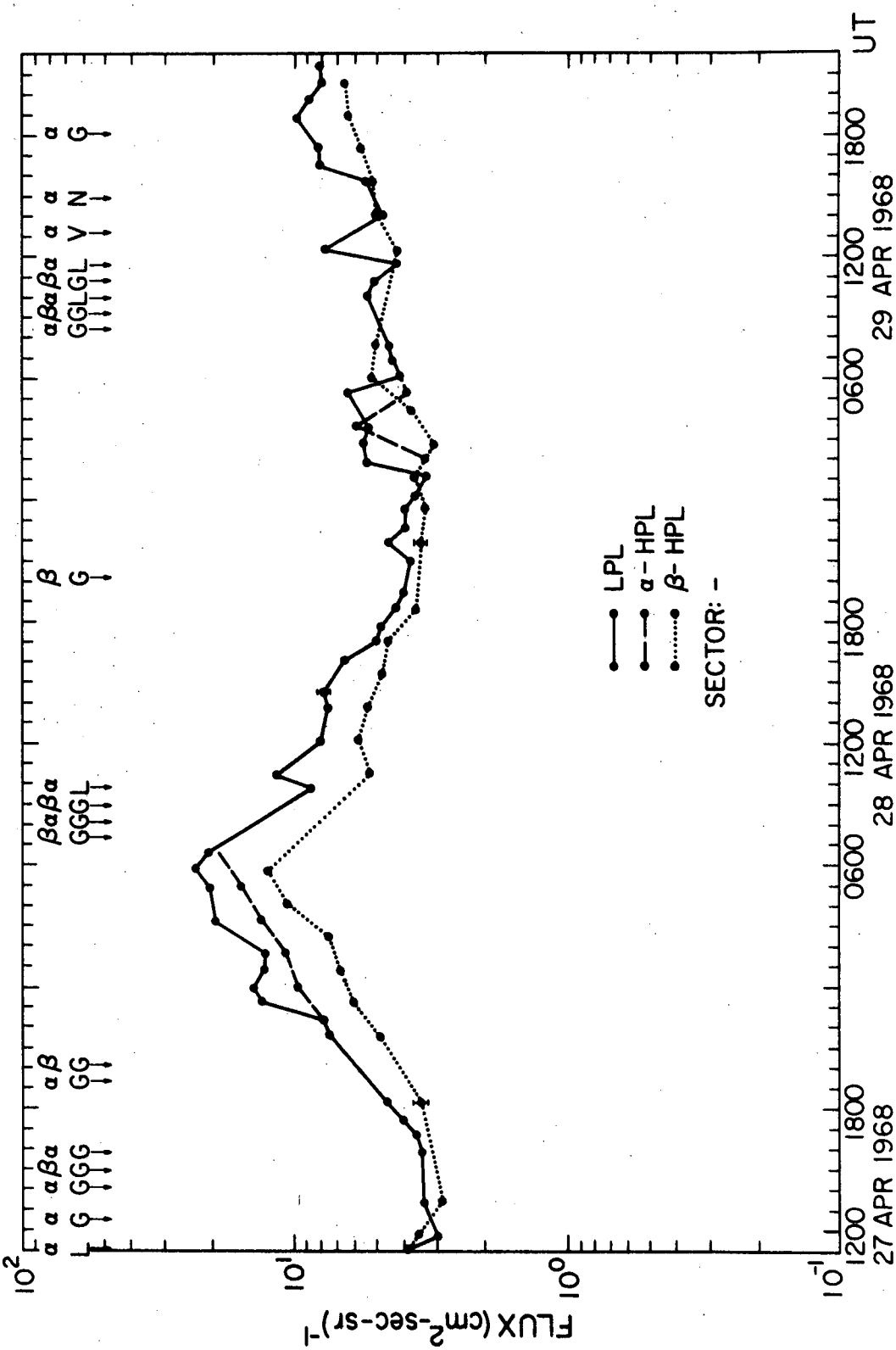
FLUX (cm²-sec-sr)⁻¹
10²
10¹
10⁰
10⁻¹
α α αβα αβ βαβα β αβαβα α α α
L G GGG GG GGGL G GGLGL V N G
1200 1800 0600 1200 1800 0600 1200 1800
27 APR 1968 28 APR 1968 29 APR 1968
UT
LPL
α - HPL
β - HPL
SECTOR: -

Figure A-11

13 May 1968 -- Solar Flare Event

1. An example of a persistent β-HPL enhancement. This feature lasts for ∿40 hours. A small increase (probably an EDP event) is superimposed on the LPL flux and α-HPL flux near the beginning of the profile.

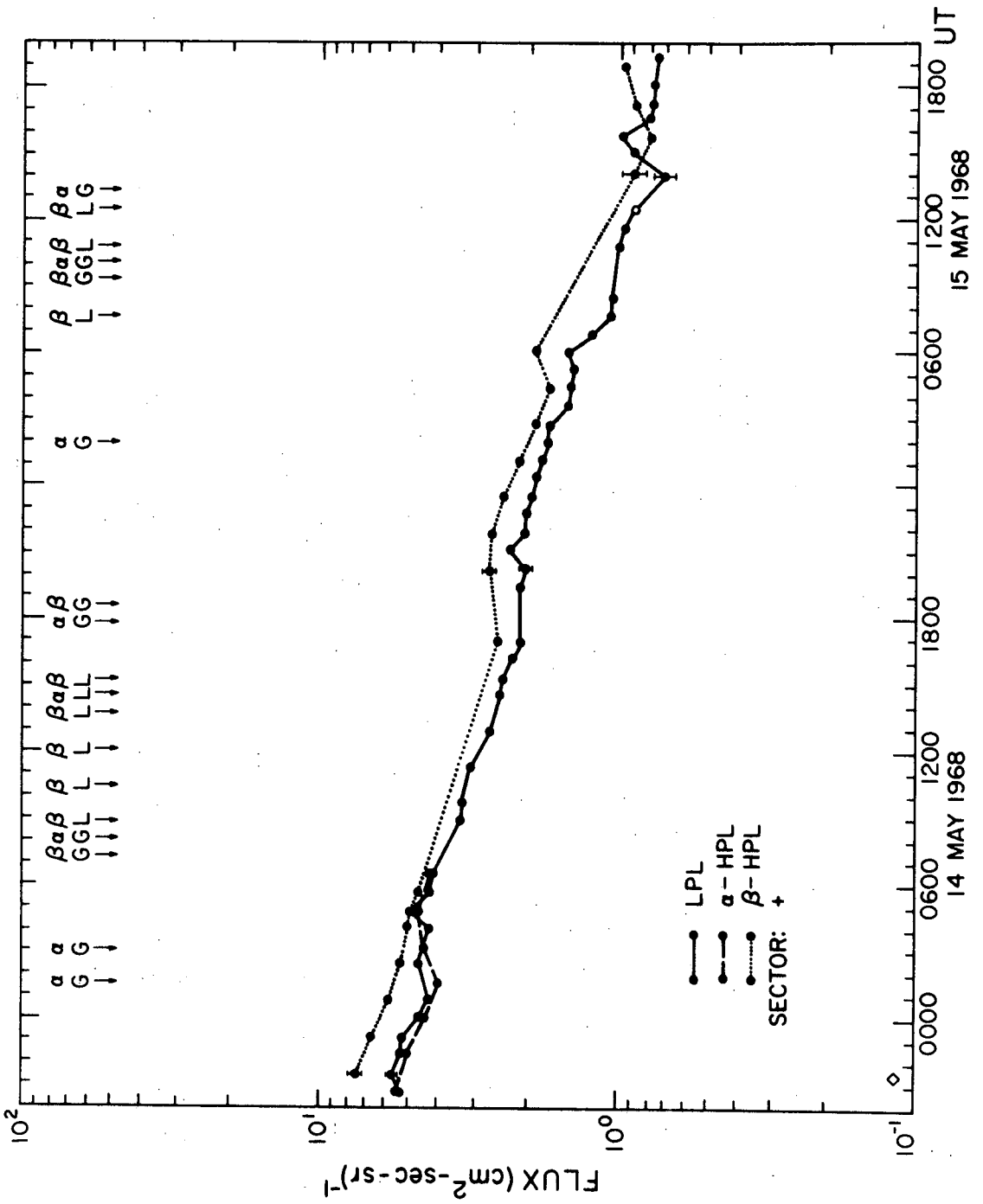
α α
G G
βαβ β β βαβ αβ α β βαβ βα
GGL L L LLL GG G L GGL LG
LPL
α – HPL
β – HPL
SECTOR: +
FLUX (cm²-sec-sr)⁻¹
10²
10¹
10⁰
10⁻¹
0000
0600
1200
1800
0600
1200
1800
14 MAY 1968
15 MAY 1968
UT

Figure A-12

13 July 1968 -- Solar Flare Event

1. Flux levels are very high on these rates, and errors are consequently very small.

2. The temporary disappearance of the persistent β-HPL feature between ∿0700 UT and ∿0840 UT on 13 July is probably related to the period of uncertain sector structure near ∿0730 UT.

3. After ∿0840 UT on 13 July the β-HPL flux decayed for ≥5 hours while the LPL and α-HPL fluxes were increasing.

4. The small increase in the β-HPL flux at ∿1500 UT on 13 July might be associated with the increase seen at LPL at ∿1100 UT.

5. The most notable feature of this profile is the event which reaches a maximum flux at ∿1800 UT on 13 July at LPL. The following observations can be made about this event:

    a. The gap in the LPL and α-HPL fluxes at ∿1900 UT is due to overscaling (see Section IV).

    b. The event reaches a maximum at β-HPL ∿3 hours later than at LPL. The maximum flux is lower, and the "width" of the peak is much greater.

    c. The transition from β-HPL depression to β-HPL enhancement

occurs prior to the β-HPL peak.

d. During the decay of this event the β-HPL flux remains greater than the LPL and α-HPL fluxes, with the exception of the broad feature (EDP?) superimposed on the decay from ∿0400 UT to ∿1400 UT on 14 July.

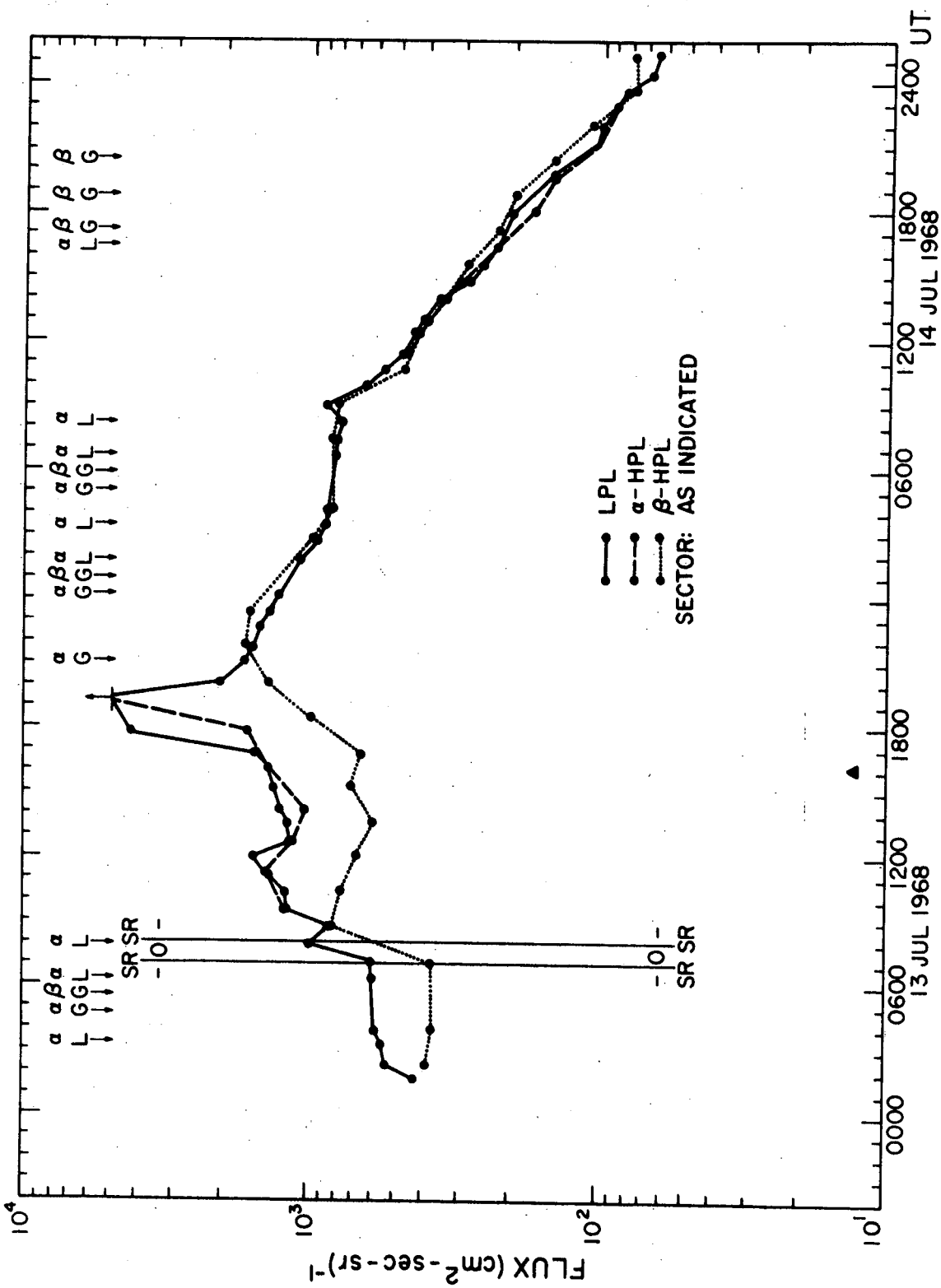
FLUX (cm²-sec-sr)⁻¹
10⁴
10³
10²
10¹
0000
0600
1200
1800
13 JUL 1968
0600
1200
1800
2400
14 JUL 1968
UT
LPL
α-HPL
β-HPL
SECTOR: AS INDICATED
SR SR
SR SR
α αβα α
L GGL L
α αβα α αβα α
G GGL L GGL L
αβ β β
LG G G

APPENDIX B

Particle Trajectories in a Turning Magnetic Field

The configuration of the geomagnetic field in the presence of significant merging between the geomagnetic and interplanetary magnetic fields has been the subject of a good deal of effort on the part of several investigators (see Sections VI and VII and the pertinent references cited therein). The access of charged particles into the magnetosphere with such a configuration is rather straightforward: the direct connection between the fields implies that trajectories probably exist whereby particles in interplanetary space can more or less "follow" the field lines into the geomagnetic tail. The assumption which is normally made is that these interplanetary particles gain access to the geomagnetic tail adiabatically, which means that the magnetic moment is conserved and that consequently the pitch angle of the particle in the tail, ϕ_{gt}, is related to that in interplanetary space, ϕ_{ip}, by

$$\sin^2(\phi_{gt}) = \frac{B_{gt}}{B_{ip}} \sin^2(\phi_{ip}) \qquad (B.1)$$

where B_{gt} and B_{ip} represent the magnitude of the geomagnetic field and the interplanetary magnetic field, respectively.

One of the implications of the assumption summarized in (B.1) is that the particles observed over one polar cap will be those whose interplanetary pitch angles were $\leq 1^{o}$, while the particles observed over the other polar cap will be those whose pitch angles in interplanetary space

were $\gtrsim 179^{\circ}$. The interplanetary pitch angles observed at a given pole would be dependent on the sector of the interplanetary field: a detector in the northern polar region would observe $\phi_{ip} \simeq 0^{\circ}$ particles during a positive sector and $\phi_{ip} \simeq 180^{\circ}$ particles during a negative sector. Although unimportant if the interplanetary flux is isotropic, the implications of the assumption of adiabatic motion are very significant in the presence of large interplanetary anisotropies: one would expect the differences between the fluxes observed in the two polar regions to follow a field-directed interplanetary anisotropy rather closely.

The mapping of interplanetary pitch angles onto the polar caps will be altered, however, if the assumption of adiabatic motion is relaxed. In order to simplify the following discussion, we will refer to the scale over which the magnetic field is changing direction in terms of the radius of curvature of a typical line of force for this field: i.e., the more rapidly the field changes direction the smaller the radius of curvature would be. In the limit of a minimum radius of curvature which is much larger than the gyroradius of the particles, one would expect adiabatic motion to be a rather good approximation. The gyroradius of a 1 MeV proton in a 50 μG interplanetary field is, however, 6.8 $R_{\oplus}$, while that for a 10 MeV proton is 21.5 $R_{\oplus}$. Since the geomagnetic tail itself has a radius of about 20-30 $R_{\oplus}$, adiabatic motion may require a transition region between the interplanetary field and the geomagnetic field of 70-220 $R_{\oplus}$. In order to place constraints on the size of this transition region based on particle observations in the polar cap regions and in interplanetary space in the presence of large interplanetary anisotropies,

Figure B-1

Schematic representation of a "turning" magnetic field.

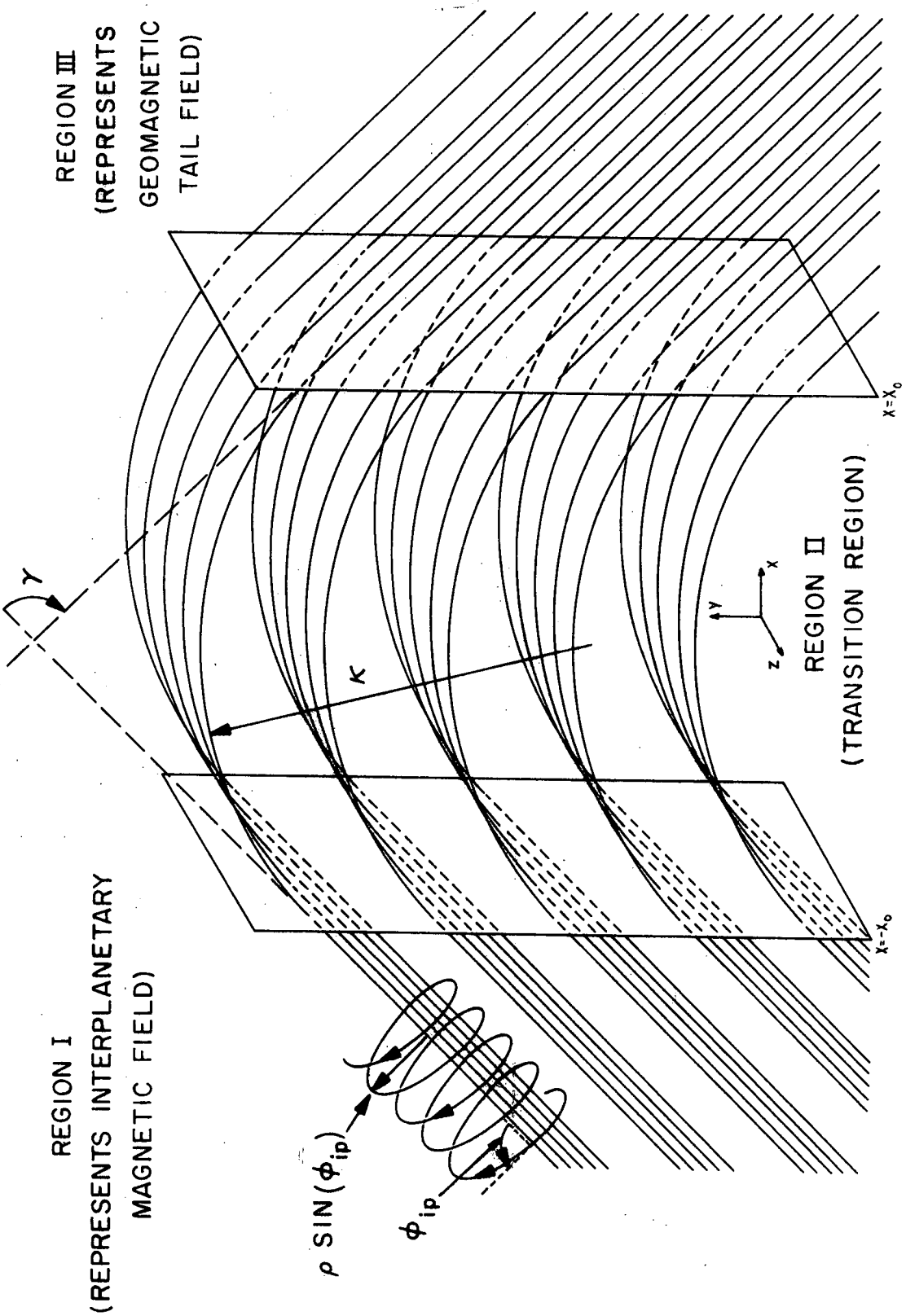
REGION III
(REPRESENTS
GEOMAGNETIC
TAIL FIELD)
REGION I
(REPRESENTS INTERPLANETARY
MAGNETIC FIELD)
REGION II
(TRANSITION REGION)
γ
κ
ρ SIN(φip)
φip
X=X0
X=-X0
Y
X
Z

it is necessary to investigate this problem in more detail.

A good deal of insight into the pitch angle mapping problem can be gained by analyzing the behavior of particles in the field configuration illustrated in figure B-1: two regions, each containing a uniform, homogeneous magnetic field of the same magnitude, separated by a transition region in which the constant magnitude field changes direction (in the plane of the two fields only) at a constant rate (i.e., the radius of curvature, κ, of a line of force in this region is a constant throughout the region). The total angle through which the field turns is designated by γ. The equation of motion of a proton in such a field is given by the Lorentz force:

$$\frac{d\vec{v}}{dt} = \frac{e}{mc}(\vec{v} \times \vec{B}) \tag{B.2}$$

The solutions of this equation in Regions I and III are helices whose axes are parallel to the magnetic field. In region III this is given by

$$\begin{aligned} x &= [v\cos(\phi)\cos(\beta)]t + \rho\sin(\phi)\sin(\beta)\cos(\omega t+\delta) \\ &\qquad + [x_0 - \rho\sin(\phi)\cos(\delta)\sin(\beta)] \\ y &= \rho\sin(\phi)[\cos(\omega t+\delta)-\cos(\delta)]\cos(\beta)-[v\cos(\phi)\sin(\beta)]t+y_0 \\ z &= \rho\sin(\phi)[\sin(\omega t+\delta)-\sin(\delta)]+z_0 \end{aligned} \tag{B.3}$$

and

$$v_x = v[\cos(\phi)\cos(\beta)+\sin(\phi)\sin(\beta)\sin(\omega t+\delta)]$$
$$v_y = v[\sin(\phi)\cos(\beta)\sin(\omega t+\delta)-\cos(\phi)\sin(\beta)] \qquad (B.4)$$
$$v_z = v\ \sin(\phi)\cos(\omega t+\delta)$$

where β is the angle between the field and the x-axis, ϕ is the pitch angle of the particle, ρ is the gyroradius of the particle, and x_o, y_o, z_o and δ specify the initial position of the particle and phase of its motion. An almost identical set of equations can be written for the solution in region I. These equations can be used to determine whether a proton which is leaving region II will re-enter region II and, if so, where and with what velocity. The situation within region II is, on the other hand, completely different: (B.2) is no longer amenable to an analytic solution, but the computational simplicity of (B.2) makes the use of a digital computer natural.

Using the techniques outlined above, a digital computer was programmed to determine charged particle trajectories in the magnetic field configuration shown in figure B-1. Since the motion of the particles after they have gained access to the geomagnetic tail is assumed to be adiabatic, the particles observed at the orbit of a low altitude, polar orbitting satellite will have had pitch angles very near 0° (north pole) or 180° (south pole) in the geomagnetic tail near the access windows. The problem was therefore delimited to one of finding the interplanetary

(region I) pitch angle, ϕ_{ip}, which would result in a 0° pitch angle in the northern geomagnetic tail (region III) for various values of the pertinent parameters. Solutions for the southern geomagnetic pole can be obtained by taking the supplement of the pitch angle found for the northern tail.

Figures B-2 and B-3 show typical results from these calculations. Figure B-2 shows ϕ_{ip} as a function of κ/ρ for five values of γ, where κ is the radius of curvature of the field, and ρ is the gyroradius of the particle. Figure B-3 shows ϕ_{ip} as a function of γ for six values of κ/ρ. It is interesting that for a configuration in which the field is turning too sharply (κ/ρ small), no interplanetary particles are seen at the polar caps if $\gamma \gtrsim 90^{\circ}$.

It is immediately obvious from figures B-2 and B-3 that the mapping of interplanetary pitch angle distributions into particles observed over the polar caps is by no means a simple one. From these data one can generate contours of the minimum κ/ρ and the maximum γ which insure that a given interplanetary pitch angle will be observable over the polar caps. Such contours are presented in figure B-4. Contours such as these can be used in conjunction with polar cap and interplanetary pitch angle distribution observations to place constraints on the magnetic field configuration in the access window region. Suppose, for instance, that it were established from observations that only those protons with interplanetary pitch angles $\lesssim 4^{\circ}$ were observed in one polar cap, while only those with interplanetary pitch angles $\gtrsim 176^{\circ}$ were observed in the other polar cap.

Figure B-2

Interplanetary pitch angles giving a 0° pitch angle in the northern geomagnetic tail as a function of the radius of curvature, κ, of the field in the transition region (see figure B-1) and the gyroradius, ρ, of the particle. Results are shown for five different field configurations, represented by different angles, γ, through which the field turns.

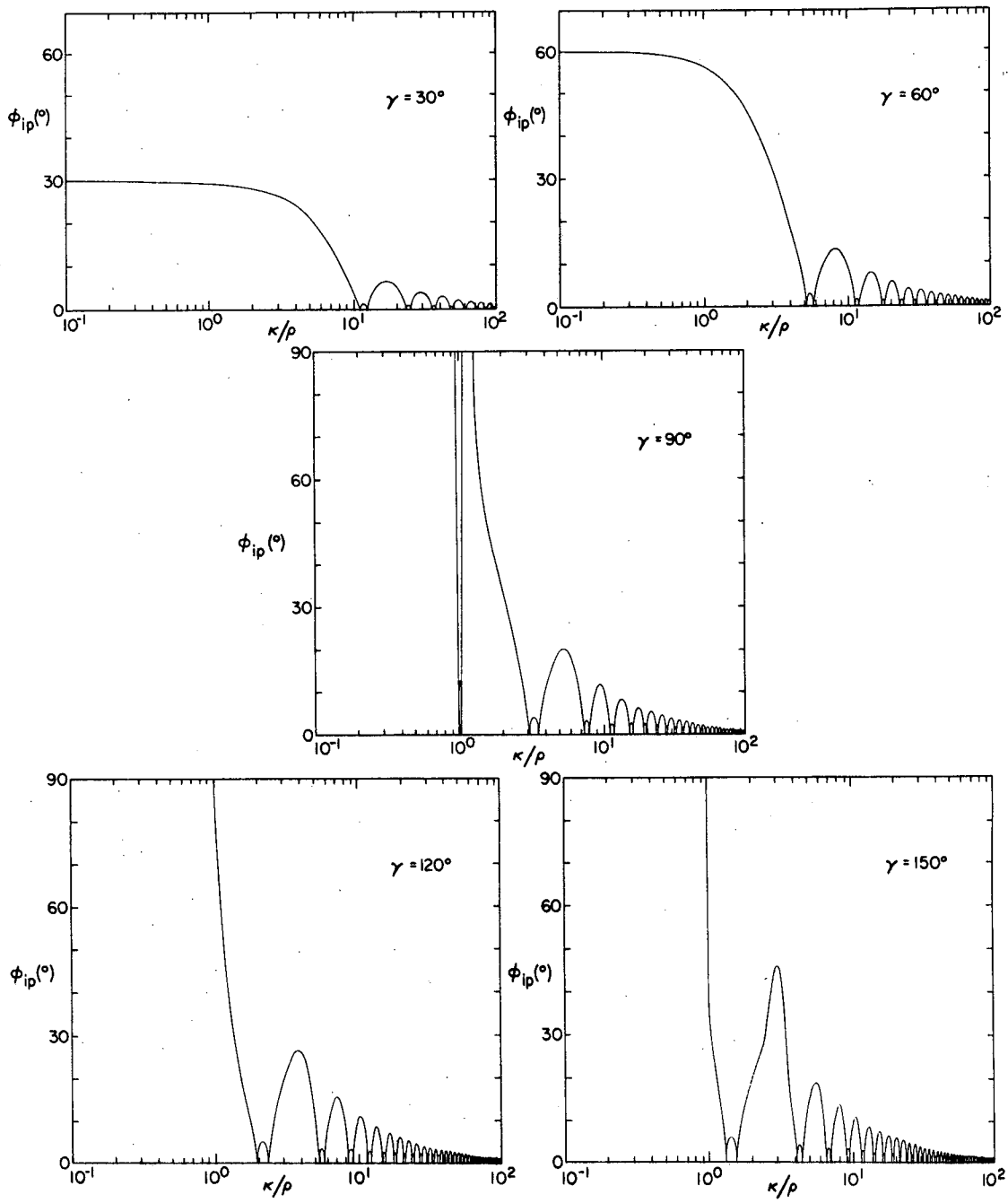
γ = 30°
γ = 60°
γ = 90°
γ = 120°
γ = 150°
ϕ_{ip}(°)
κ/ρ
10^{-1}
10^{0}
10^{1}
10^{2}
0
30
60
90

Figure B-3

Interplanetary pitch angles giving a 0° pitch angle in the northern geomagnetic tail as a function of the angle, γ, through which the magnetic field turns (see figure B-1). Results are shown for six values of κ/ρ.

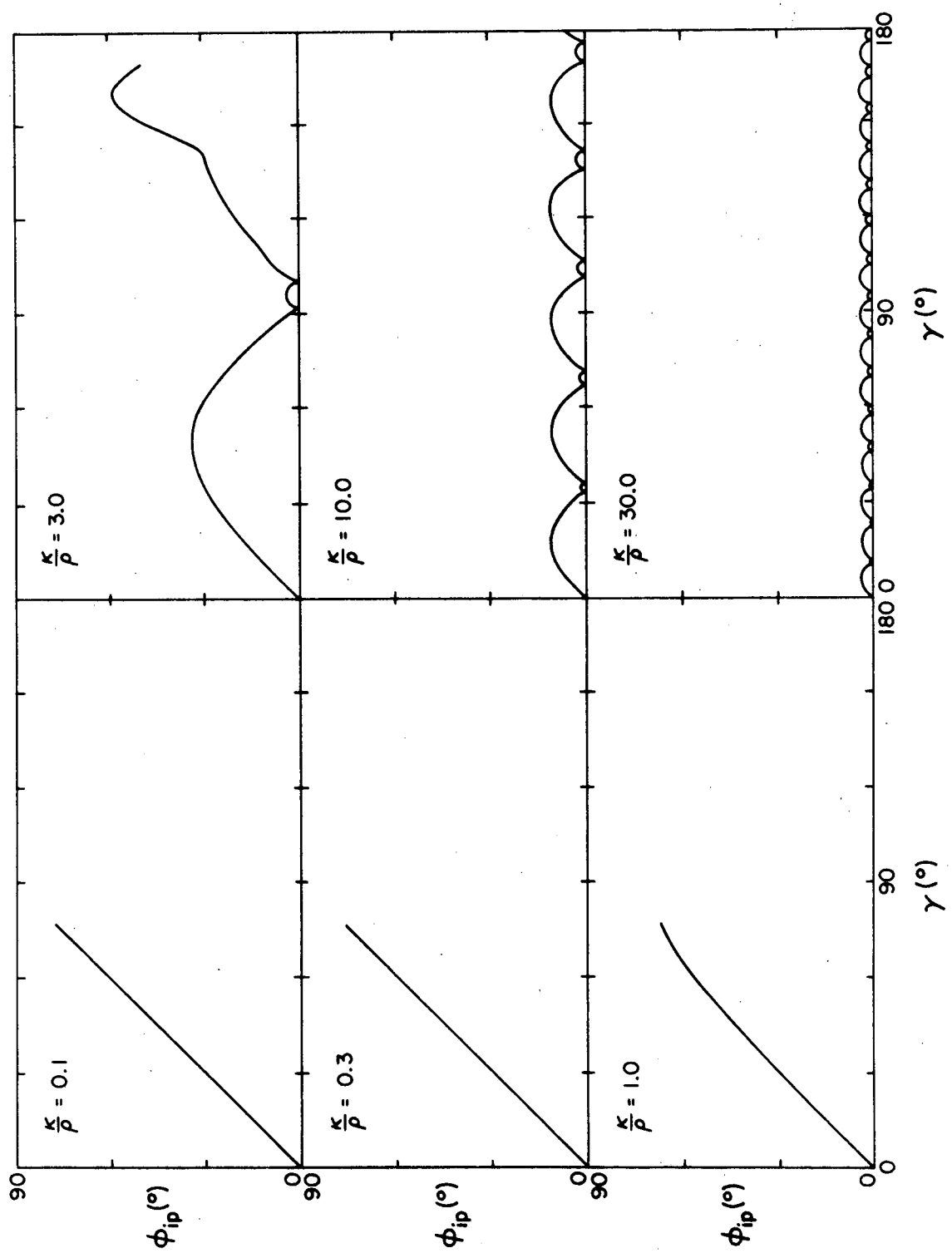
$\frac{K}{\rho}$ = 0.1
$\frac{K}{\rho}$ = 0.3
$\frac{K}{\rho}$ = 1.0
$\frac{K}{\rho}$ = 3.0
$\frac{K}{\rho}$ = 10.0
$\frac{K}{\rho}$ = 30.0
ϕ_{ip} (°)
90
0
γ (°)
0
90
180

Figure B-4

Contours of the minimum κ/ρ for a given value of γ (or maximum γ for a given value of κ/ρ) which will insure that the particles observed in the polar cap region represent interplanetary pitch angles no greater than the specified values.

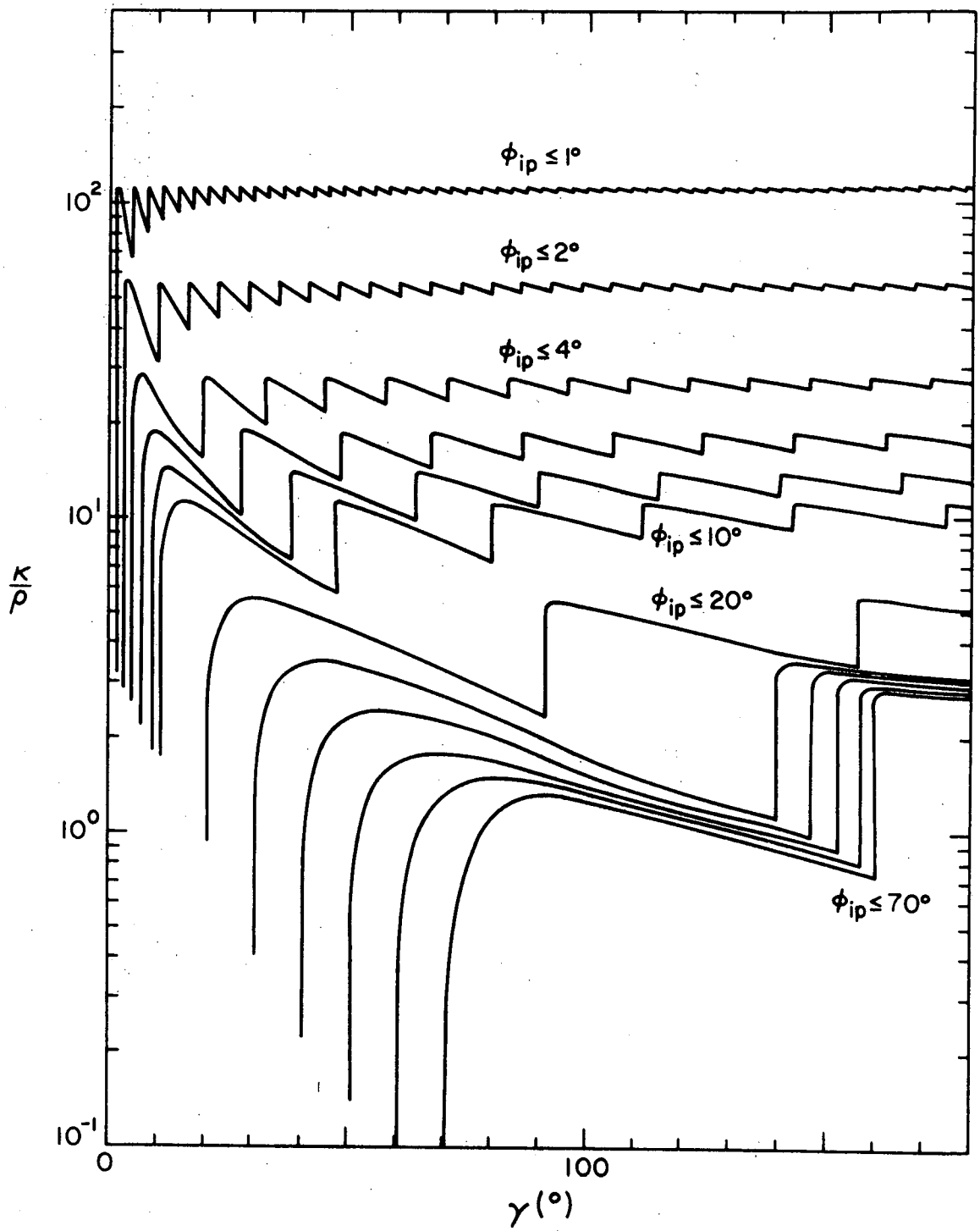
$\phi_{ip} \leq 1°$
$\phi_{ip} \leq 2°$
$\phi_{ip} \leq 4°$
$\phi_{ip} \leq 10°$
$\phi_{ip} \leq 20°$
$\phi_{ip} \leq 70°$
10^2
10^1
10^0
10^{-1}
$\frac{\kappa}{\rho}$
0
100
γ (°)

Considering that the field will "turn" through an average angle of either 48° or 132° (48° is the average Archimedian spiral angle at 1 AU, while the geomagnetic tail field is either parallel or antiparallel to the solar wind, which flows radially away from the sun), then the $\phi_{ip} \leq 4°$ contour on figure B-4 would imply that we must have $\kappa \geq 27$ for the transition regions for both poles. For 1 MeV protons, this means $\kappa \geq 184\ R_\oplus$ (1.17×10^6 km), while for 10 MeV protons this means $\kappa \geq 580\ R_\oplus$ (3.7×10^6 km). For comparison, the tail, itself, is probably 40-60 $R_\oplus$ in diameter (see the discussion by Evans [101] for a more detailed consideration of the tail size and shape).

APPENDIX C

Magnetic Merging at the Polar Neutral Points

Frank [4] has recently proposed a magnetospheric model (see Section VII) which is of special interest to the study of low rigidity particle access to the polar regions: a direct consequence of the model is the possible formation of geomagnetic tails of different lengths for the two polar regions. It is the purpose of the study presented in this appendix to investigate the mechanisms which give rise to this consequence with a view toward determining what constraints must be placed on the model in order to yield the $L\alpha\beta$ access window configuration discussed in Section VII.

The major assumption of this model is the postulation that all merging between the geomagnetic field and the interplanetary magnetic field occurs at the polar neutral points. The location of these neutral points with respect to the magnetosphere is indicated in figure VI-5. Both open and closed geomagnetic field lines are assumed to merge with the interplanetary field at the neutral points, but the lines which were originally closed subsequently remerge in the neutral sheet. Since the interplanetary field lines with which open geomagnetic field lines merge are convected away from the earth with the solar wind, the length of the geomagnetic tail is proportional to its "age" (i.e., the time required for these open field lines to complete one cycle from merging to merging again). This age is, in turn, inversely proportional to the rate at which open field lines merge at the appropriate polar neutral point. In order to evaluate this model with respect to observational results, it

is necessary to investigate this merging process and the relative open field line merging rates at the two poles in some detail.

Assumptions

The field configuration at the polar neutral point is represented in figure C-1, which shows the geomagnetic field at the northern neutral point, over which the interplanetary magnetic field has been pulled by the solar wind. The geometry of the field clearly contributes greatly to the complexity of the problem in this configuration. It is sufficient at this point, though, to consider the plane configuration shown in figure C-2, which may be related to the more complex geometry by considering the situation in the immediate vicinity of the neutral point in figure C-1. These figures can be transformed into a representation of the southern polar neutral point by reversing the sense of the geomagnetic field.

Figure C-2 also illustrates two of the parameters which will be used in this study:

ϕ: the angle between a field line and the projection of the earth-sun line in the plane of the field interface, measured from the anti-solar direction.

ψ: the angle between a given geomagnetic field line and the direction of the interplanetary magnetic field.

This study is predicated on the following assumptions:

1. The boundary between open and closed geomagnetic field lines

Figure C-1

Schematic representation of the field configuration at the northern polar neutral point. A possible configuration for the interplanetary magnetic field near the neutral point is indicated by the heavier lines.

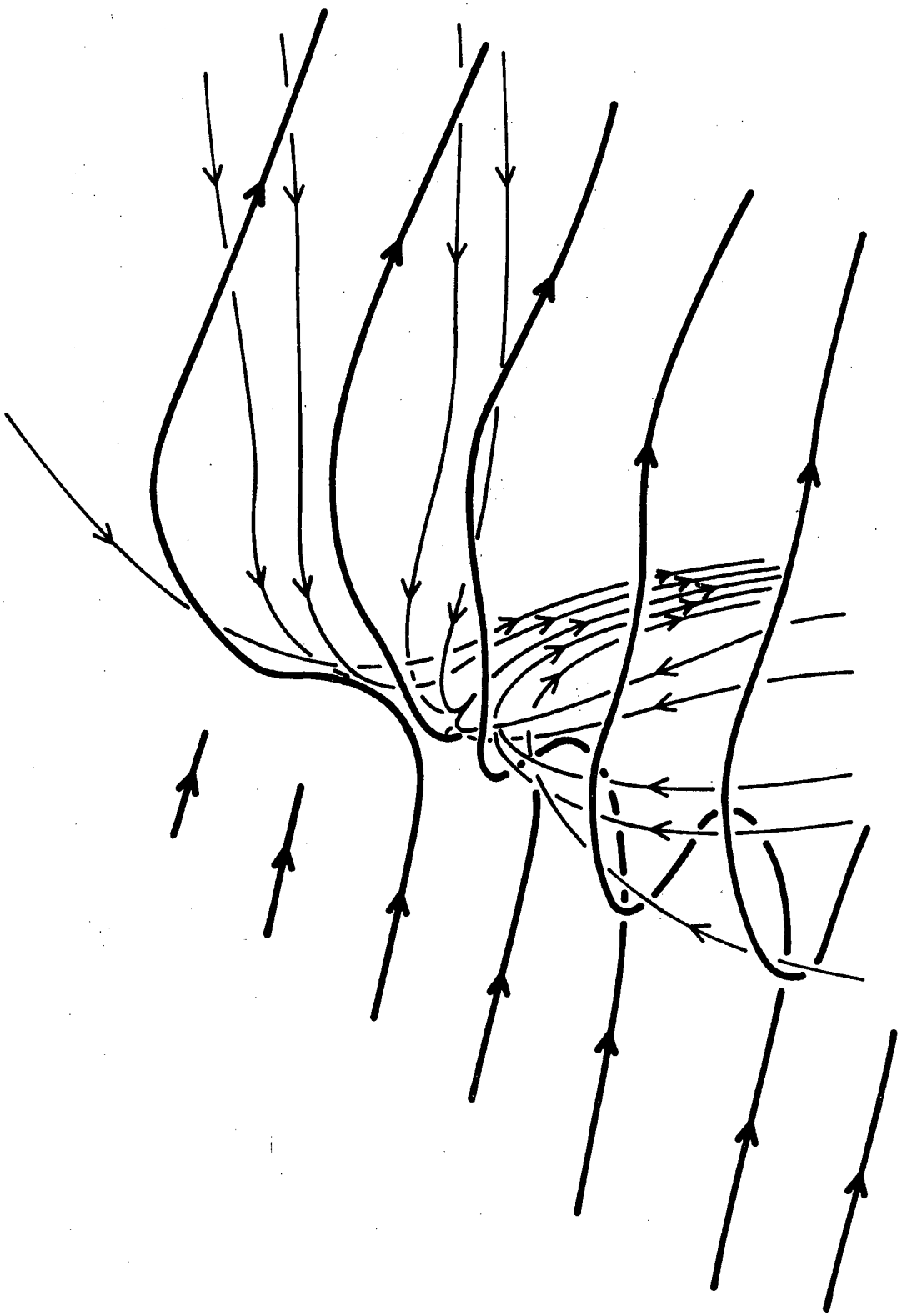

C.2

Figure C-2

Schematic representation of a plane interface between a uniform magnetic field and a magnetic field with a neutral point. This field configuration is essentially the same as that shown in figure C-1, while the geometry is greatly simplified.

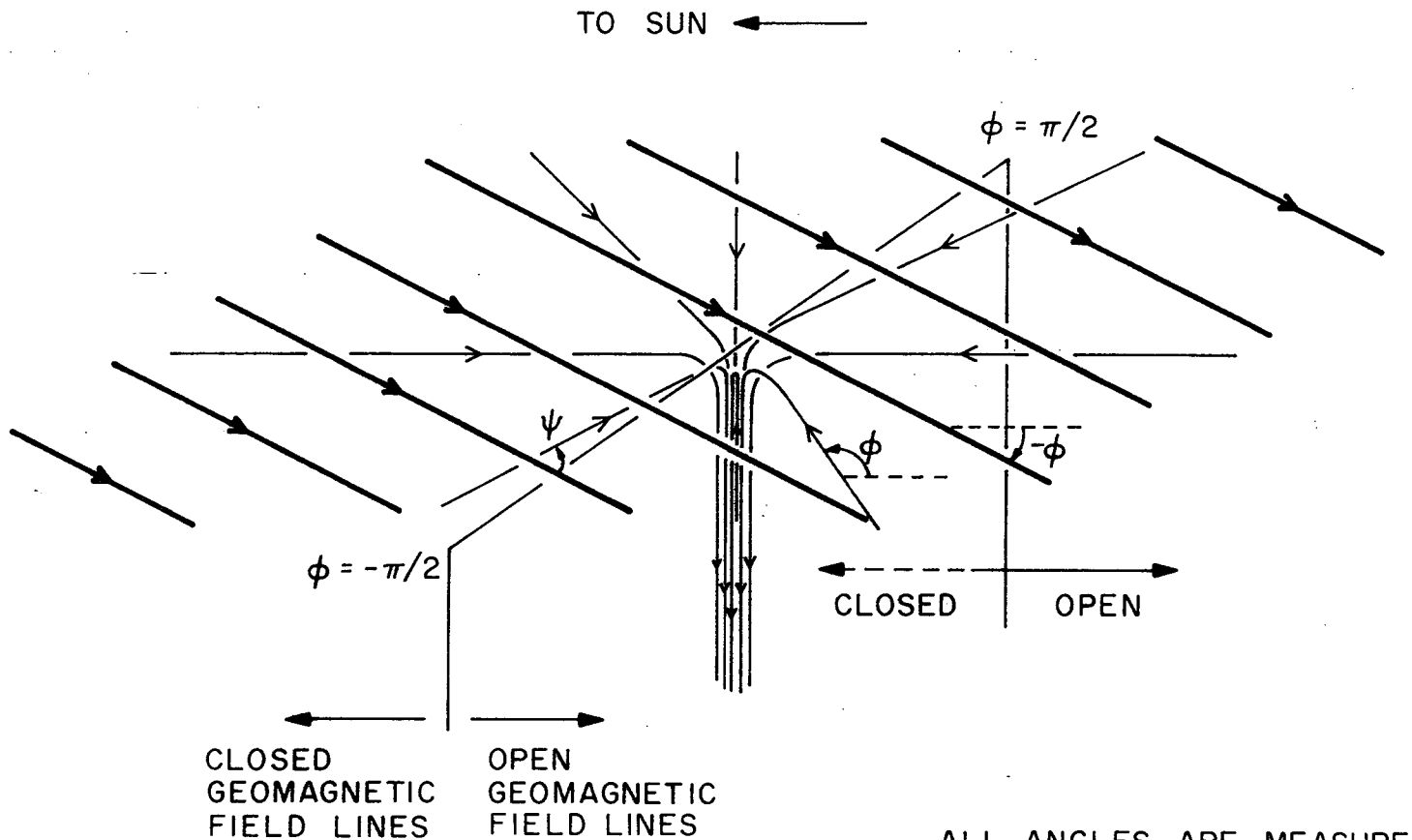

ALL ANGLES ARE MEASURED IN A PLANE PARALLEL TO PLANE OF INTERFACE BETWEEN THE TWO FIELDS

is assumed to be perpendicular to the earth-sun line, with open field lines being those lines with ϕ in the interval $[-\pi/2,\pi/2)$.

2. The angular configuration of the interplanetary magnetic field in the plane of the interface between the two fields is assumed to vary randomly, over a period of a few hours, according to a Gaussian-like distribution:

$$P(\phi) = \frac{C}{\sigma\sqrt{(2\pi)}} e^{-(\phi-\Phi)^2/2\sigma^2} \tag{C.1}$$

where C is defined by normalization:

$$\int_{-\pi}^{\pi} d\phi \; P(\phi) = 1 \tag{C.2}$$

which implies

$$C = \left[\mathrm{erf}\left(\frac{\pi}{\sigma\sqrt{(2)}}\right)\right]^{-1} \tag{C.3}$$

3. The rate at which a given geomagnetic field line merges with the interplanetary magnetic field is dependent only on the solar wind velocity, the maximum merging rate for *any* two field lines based on plasma parameters, and the angle, ψ, between the geomagnetic field line in question and the direction of the interplanetary field.

4. The rate at which plasma is supplied for the merging process is limited by the solar wind velocity in the vicinity of the neutral point.

5. The rate at which the interplanetary field merges is the same at both polar neutral points.

Since the interplanetary field is "frozen into" the solar wind plasma, magnetic merging rates can be expressed in terms of equivalent plasma velocities. This equivalence conforms to the nomenclature used by Petschek [e.g. 86], Sonnerup [87], and Yeh and Axford [88]. One of the results of these previous studies which is of most significance here is the determination of the maximum equivalent plasma velocity, U_m. There is some disagreement, however, as to the proper dependence of U_m on plasma parameters:

$$U_m = \frac{V_A \pi}{4 \ln\left(\frac{16 U_m^2 \pi \sigma L}{V_A c^2}\right)} \qquad \text{(Petschek)}$$

$$U_m = V_A[1+\sqrt{(2)}] \qquad \text{(Sonnerup)} \qquad \text{(C.4)}$$

$$U_m < \infty \qquad \text{(Yeh and Axford)}$$

Without attempting to choose among these, we will express our results relative to U_m. Although all of these studies have dealt with the configuration of exactly anti-parallel fields, the results are applicable to the present configuration if the fields which are at an angle ψ to each other are resolved into parallel and anti-parallel components. Since the superposition of a constant magnetic field perpendicular to the antiparallel fields considered in the above studies has no essential effect on their derivations, we can write the maximum possible merging rate for fields at an angle ψ as

$$U_{max}(\psi) = U_m \sin(\psi/2) \tag{C.5}$$

so that the actual merging rate for these fields obeys

$$u(\psi) \in [0, U_{max}(\psi)] \tag{C.6}$$

The only other information available about the form of $u(\psi)$ is the normalization implied by the fourth assumption above:

$$2\int_0^{\pi} d\psi\, u(\psi) \leq V_{sw} \tag{C.7}$$

As a consequence, the specification of an exact form for $u(\psi)$ in the case of V_{sw}/U_m sufficiently small is somewhat arbitrary. The question, of course, is whether the interplanetary magnetic field merges preferentially with more nearly antiparallel geomagnetic field lines. Since the answer to this is not clear, three assumptions will be made about the angular dependence of the merging rate, each of which will, of course, lead to different results. Figure C-3 illustrates the general form taken by $u(\psi)$ under each of these assumptions.

Assumption A

The probability that two field lines will merge is taken to be independent of the angle between them. This means

Figure C-3

General behavior of $u(\psi)$ for each of the three assumptions made in the text.

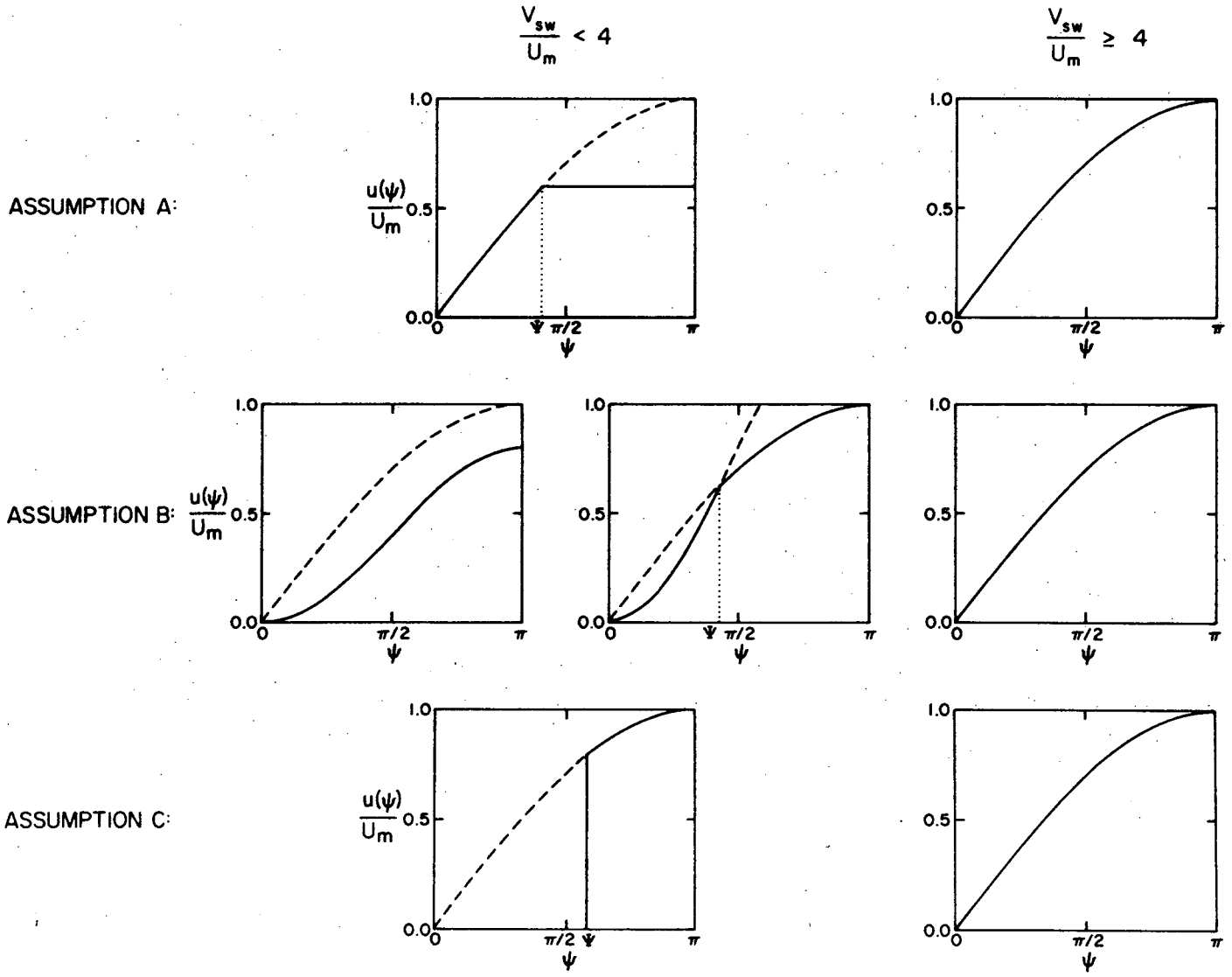
$\frac{V_{sw}}{U_m} < 4$
$\frac{V_{sw}}{U_m} \geq 4$
ASSUMPTION A:
ASSUMPTION B:
ASSUMPTION C:
$\frac{u(\psi)}{U_m}$
1.0
0.5
0.0
0
$\pi/2$
π
ψ

$$u(\psi) = U_m \sin(\psi/2) \quad ; \quad \psi < \Psi$$
$$= U_m \sin(\Psi/2) \quad ; \quad \psi \geq \Psi \tag{C.8}$$

where Ψ is determined by the normalization given by (C.7), which gives

$$(\pi-\Psi)\sin(\Psi/2)+2[1-\cos(\Psi/2)] = V_{sw}/2U_m \quad ; \quad V_{sw}/U_m \leq 4$$
$$\Psi = \pi \quad ; \quad V_{sw}/U_m > 4 \tag{C.9}$$

Assumption B

Under this assumption, the likelihood that two field lines will merge is assumed to be a function of the angle between them, with the likelihood varying directly with the angle. Since the choice of this function is at this point completely arbitrary, however, the merging likelihood will be chosen to be proportional to $\sin(\psi/2)$ in order to take advantage of the consequent simplifications in the derivations to follow. Hence we have

$$u(\psi) = \frac{V_{sw}}{\pi} \sin^2(\psi/2) \quad ; \quad V_{sw}/U_m \leq \pi$$

$$= U_m \sin^2(\psi/2) \,/\, \sin(\Psi/2) \quad ; \quad \psi < \Psi \quad \Big\} \; V_{sw}/U_m > \pi$$

$$= U_m \sin(\psi/2) \quad ; \quad \psi \geq \Psi \quad \Big\} \tag{C.10}$$

where, from (C.7), Ψ is given by

$$\frac{\Psi + \sin(\Psi)}{\sin(\Psi/2)} = \frac{V_{sw}}{U_m} \quad ; \quad \pi < V_{sw}/U_m \leq 4$$
$$\Psi = 0 \quad ; \quad V_{sw}/U_m > 4 \tag{C.11}$$

Assumption C

For this case it is assumed that the interplanetary field will merge preferentially with the most nearly antiparallel geomagnetic field available. This assumption, which is the converse of Assumption A, yields

$$u(\psi) = 0 \quad ; \quad \psi < \Psi$$
$$= U_m \sin(\psi/2) \quad ; \quad \psi \geq \Psi \tag{C.12}$$

and (C.7) yields the following definition of Ψ:

$$\Psi = 2\cos^{-1}\left(\frac{V_{sw}}{4U_m}\right) \quad ; \quad V_{sw}/U_m \leq 4$$
$$\Psi = 0 \quad ; \quad V_{sw}/U_m > 4 \tag{C.13}$$

The solutions for Ψ from (C.9), (C.11), and (C.13) are shown in figure C-4.

Derivation of Merging Rates -- General

We will now define the following symbolism:

U_{ON} = merging velocity for open field lines at the northern polar neutral point

U_{CN} = merging velocity for closed field lines at the northern polar neutral point

U_{OS} = merging velocity for open field lines at the southern polar neutral point

U_{CS} = merging velocity for closed field lines at the southern polar neutral point

From the symmetry implied from the assumption that the boundary between open and closed field lines at the neutral point is the plane through the neutral point and perpendicular to the projection of the earth-sun line into the plane of the field interface (see figure C-2), and the assumption that $U_{ON}+U_{CN} = U_{OS}+U_{CS}$, we have

$$U_{ON} = U_{CS}$$
$$U_{OS} = U_{CN} \qquad \text{(C.14)}$$

Concentrating our attention on U_{ON} and U_{OS}, then, we can write

Figure C-4

Critical angle, Ψ, as a function of V_{sw}/U_m for each of the three assumptions made in the text.

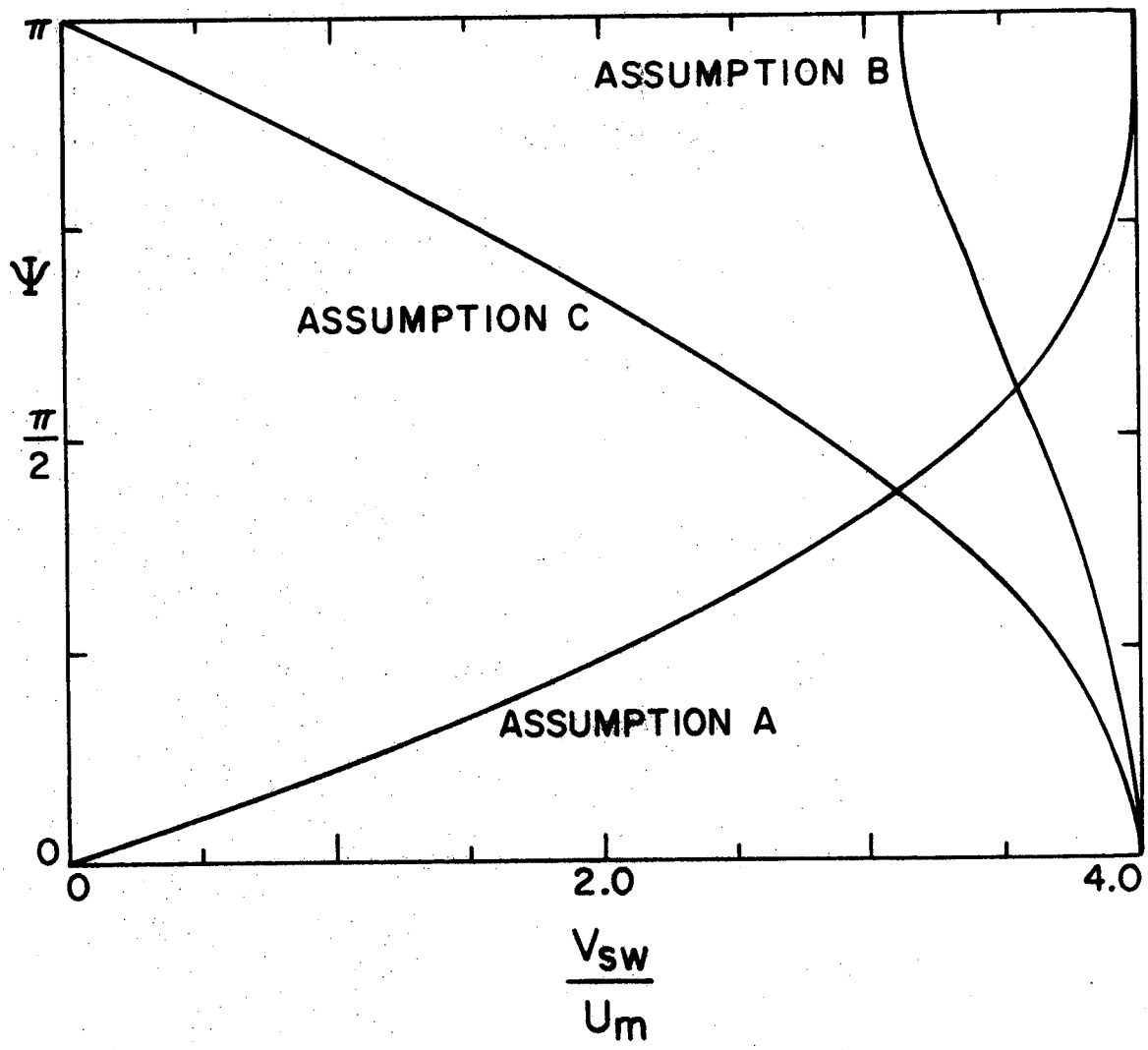
π
Ψ
π/2
0
0
2.0
4.0
ASSUMPTION B
ASSUMPTION C
ASSUMPTION A
Vsw/Um

Case I: $\Phi \in [-\pi/2,\pi/2]$:

$$U^{I}_{Op}(\Phi,\sigma) = \int_{\Phi-\pi}^{-\pi/2} d\phi\ P(\phi)\upsilon_{Op1}(\phi) + \int_{-\pi/2}^{\pi/2} d\phi\ P(\phi)\upsilon_{Op2}(\phi)$$

$$+ \int_{\pi/2}^{\Phi+\pi} d\phi\ P(\phi)\upsilon_{Op3}(\phi) \quad ; \quad p=N,S \qquad (C.15)$$

Case II: $\Phi \in [\pi/2,3\pi/2]$:

$$U^{II}_{Op}(\Phi,\sigma) = \int_{\Phi-\pi}^{\pi/2} d\phi\ P(\phi)\upsilon_{Op2}(\phi) + \int_{\pi/2}^{3\pi/2} d\phi\ P(\phi)\upsilon_{Op3}(\phi)$$

$$+ \int_{3\pi/2}^{\Phi+\pi} d\phi\ P(\phi)\upsilon_{Op4}(\phi) \quad ; \quad p=N,S \qquad (C.16)$$

where the $\upsilon_{Opi}(\phi)$ are given by

$$\upsilon_{ON1}(\phi) = \int_{-\pi}^{-(\phi+3\pi/2)} d\psi\ |u(\psi)| + \int_{-(\phi+\pi/2)}^{\pi} d\psi\ |u(\psi)| \qquad (C.17)$$

$$\upsilon_{OS1}(\phi) = \int_{-(\phi+3\pi/2)}^{-(\phi+\pi/2)} d\psi\ |u(\psi)| \qquad (C.18)$$

$$v_{ON2}(\phi) = \int_{-\phi-\pi/2}^{-\phi+\pi/2} d\psi \ |u(\psi)| \tag{C.19}$$

$$v_{OS2}(\phi) = \int_{-\pi}^{-\phi-\pi/2} d\psi \ |u(\psi)| + \int_{-\phi+\pi/2}^{\pi} d\psi \ |u(\psi)| \tag{C.20}$$

$$v_{ON3}(\phi) = \int_{-\pi}^{-\phi+\pi/2} d\psi \ |u(\psi)| + \int_{-\phi+3\pi/2}^{\pi} d\psi \ |u(\psi)| \tag{C.21}$$

$$v_{OS3}(\phi) = \int_{-\phi+\pi/2}^{-\phi+3\pi/2} d\psi \ |u(\psi)| \tag{C.22}$$

$$v_{ON4}(\phi) = \int_{-\phi+3\pi/2}^{-\phi+5\pi/2} d\psi \ |u(\psi)| \tag{C.23}$$

$$v_{OS4}(\phi) = \int_{-\pi}^{-\phi+3\pi/2} d\psi \ |u(\psi)| + \int_{-\phi+5\pi/2}^{\pi} d\psi \ |u(\psi)| \tag{C.24}$$

In order to be able to expand the $v_{Opi}(\phi)$, it is useful to at this time introduce the following integrals which will be needed later:

$$I_0(\alpha,\beta) = \frac{1}{\sigma\sqrt{(2\pi)}} \int_\alpha^\beta d\phi \; e^{-(\phi-\Phi)^2/2\sigma^2}$$

$$= [\mathrm{erf}(b)-\mathrm{erf}(a)]/2 \qquad (C.25)$$

$$I_1(\alpha,\beta) = \frac{1}{\sigma\sqrt{(2\pi)}} \int_\alpha^\beta d\phi \; \phi \; e^{-(\phi-\Phi)^2/2\sigma^2}$$

$$= \frac{\sigma}{\sqrt{(2\pi)}} \left(e^{-a^2}-e^{-b^2}\right) + \Phi[\mathrm{erf}(b)-\mathrm{erf}(a)]/2 \qquad (C.26)$$

$$I_s(\alpha,\beta) = \frac{1}{\sigma\sqrt{(2\pi)}} \int_\alpha^\beta d\phi \; \sin(\phi/2) \; e^{-(\phi-\Phi)^2/2\sigma^2}$$

$$= \frac{e^{-\sigma^2/8}}{\sigma\sqrt{2}} \mathfrak{I}\left\{e^{i\Phi/2}[\mathrm{erf}(b-i\sigma/\sqrt{8})-\mathrm{erf}(a-i\sigma/\sqrt{8})]\right\} \qquad (C.27)$$

$$I_c(\alpha,\beta) = \frac{1}{\sigma\sqrt{(2\pi)}} \int_\alpha^\beta d\phi \; \cos(\phi/2) \; e^{-(\phi-\Phi)^2/2\sigma^2}$$

$$= \frac{e^{-\sigma^2/8}}{\sigma\sqrt{2}} \mathfrak{R}\left\{e^{i\Phi/2}[\mathrm{erf}(b-i\sigma/\sqrt{8})-\mathrm{erf}(a-i\sigma/\sqrt{8})]\right\} \qquad (C.28)$$

$$I_{c2}(\alpha,\beta) = \frac{1}{\sigma\sqrt{(2\pi)}} \int_{\alpha}^{\beta} d\phi \cos(\phi)\, e^{-(\phi-\Phi)^2/2\sigma^2}$$

$$= \frac{e^{-\sigma^2/2}}{2\sigma} \Re\left\{e^{i\Phi}[\mathrm{erf}(b-i\sigma/\sqrt{2})-\mathrm{erf}(a-i\sigma/\sqrt{2})]\right\} \qquad (C.29)$$

where

$$a = \frac{\alpha-\Phi}{\sigma\sqrt{2}} \quad ; \quad b = \frac{\beta-\Phi}{\sigma\sqrt{2}} \qquad (C.30)$$

and where

$$\mathrm{erf}(z) = \frac{2}{\sqrt{\pi}} \int_{0}^{z} dt\, e^{-t^2} \qquad (C.31)$$

is the standard error function. The approximation used to evaluate erf(x+iy) is that given by Saltzer [114]:

$$\mathrm{erf}(x+iy) = \mathrm{erf}(x) + \frac{e^{-x^2}}{2\pi x}[1 + \cos(2xy) + i\sin(2xy)]$$

$$+ \frac{2}{\pi} e^{-x^2} \sum_{n=1}^{\infty} \frac{e^{-n^2/4}}{n^2+4x^2} [f_n(x,y)+ig_n(x,y)] \qquad (C.32)$$

$$f_n(x,y) = 2x - 2x\cosh(ny)\cos(2xy) + n\sin(ny)\sin(2xy)$$

$$g_n(x,y) = 2x\cosh(ny)\sin(2xy) + n\sinh(ny)\cos(2xy)$$

The relative error in this approximation is about one part in 10^{-16}.

We must now evaluate these functions ($v_{0pi}(\phi)$) for each of the three assumed forms for $u(\psi)$.

Assumption A -- see (C.8) and (C.9)

From (C.17),

$$v^{<}_{0N1}(\phi) = \int_{-\pi}^{-(\phi+3\pi/2)} d\psi \ |u(\psi)| + \int_{-(\phi+\pi/2)}^{\pi} d\psi \ |u(\psi)|$$

$$= \left| \int_{-\pi}^{-(\phi+3\pi/2)} d\psi \ u(\psi) \right| + \left| \int_{-(\phi+\pi/2)}^{\pi} d\psi \ u(\psi) \right| \qquad (C.33)$$

$$= \int_{-\pi}^{-(\phi+3\pi/2)} d\psi \ u(\psi) + \int_{-(\phi+\pi/2)}^{\pi} d\psi \ u(\psi)$$

This can be combined with (C.8) to give, for $\Psi \leq \pi/2$,

$$\frac{v^{<}_{ONI}(\phi)}{U_m} = (-\Psi+5\pi/2)\sin(\Psi/2)-2\cos(\Psi/2)+\phi\sin(\Psi/2)$$

$$-\sqrt{2}[\sin(\phi/2)+\cos(\phi/2)] \qquad \phi \in [-3\pi/2,\Psi-3\pi/2]$$

$$= \pi\sin(\Psi/2) \qquad \phi \in (\Psi-3\pi/2,-\Psi-\pi/2] \qquad (C.34)$$

$$= (-\Psi+\pi/2)\sin(\Psi/2)-2\cos(\Psi/2)-\phi\sin(\Psi/2)$$

$$+\sqrt{2}[-\sin(\phi/2)+\cos(\phi/2)] \qquad \phi \in (-\Psi-\pi/2,-\pi/2]$$

and, for $\Psi > \pi/2$,

$$\frac{v^{>}_{ONI}(\phi)}{U_m} = (-\Psi+5\pi/2)\sin(\Psi/2)-2\cos(\Psi/2)+\phi\sin(\Psi/2)$$

$$-\sqrt{2}[\sin(\phi/2)+\cos(\phi/2)] \qquad \phi \in [-3\pi/2,-\Psi-\pi/2]$$

$$= 2[(\pi-\Psi)\sin(\Psi/2)-2\cos(\Psi/2)$$

$$-\sqrt{2}\sin(\phi/2)] \qquad \phi \in (-\Psi-\pi/2,\Psi-3\pi/2] \qquad (C.35)$$

$$= (-\Psi+\pi/2)\sin(\Psi/2)-2\cos(\Psi/2)-\phi\sin(\Psi/2)$$

$$+\sqrt{2}[-\sin(\phi/2)+\cos(\phi/2)] \qquad \phi \in (\Psi-3\pi/2,-\pi/2]$$

Similarly, from (C.18),

$$\upsilon^{<}_{OS1}(\phi) = \int_{-(\phi+3\pi/2)}^{-(\phi+\pi/2)} d\psi \; |u(\psi)|$$

$$= \int_{0}^{-(\phi+\pi/2)} d\psi \; u(\psi) + \int_{0}^{\phi+3\pi/2} d\psi \; u(\psi) \qquad \text{(C.36)}$$

which, as before, can be expanded into, for $\Psi \leq \pi/2$,

$$\frac{\upsilon^{<}_{OS1}(\phi)}{U_m} = 4-(\psi+\pi/2)\sin(\Psi/2)-2\cos(\Psi/2)-\phi\sin(\Psi/2)$$

$$+\sqrt{2}[\cos(\phi/2)+\sin(\phi/2)] \qquad \phi \in [-3\pi/2, \Psi-3\pi/2]$$

$$= 4+(\pi-2\Psi)\sin(\Psi/2)-4\cos(\Psi/2) \qquad \phi \in (\Psi-3\pi/2, -\Psi-\pi/2] \qquad \text{(C.37)}$$

$$= 4-(\Psi-3\pi/2)\sin(\Psi/2)-2\cos(\Psi/2)+\phi\sin(\Psi/2)$$

$$-\sqrt{2}[\cos(\phi/2)-\sin(\phi/2)] \qquad \phi \in (-\Psi-\pi/2, -\pi/2]$$

and, for $\Psi > \pi/2$,

$$\frac{v^{>}_{OS1}(\phi)}{U_m} = 4-(\Psi+\pi/2)\sin(\Psi/2)-2\cos(\Psi/2)-\phi\sin(\Psi/2)$$

$$+\sqrt{2}[\cos(\phi/2)+\sin(\phi/2)] \qquad \phi \in [-3\pi/2,-\Psi-\pi/2]$$

$$= 4+2\sqrt{2}\sin(\phi/2) \qquad \phi \in (-\Psi-\pi/2,\Psi-3\pi/2] \qquad (C.38)$$

$$= 4-(\Psi-3\pi/2)\sin(\Psi/2)-2\cos(\Psi/2)+\phi\sin(\Psi/2)$$

$$-\sqrt{2}[\cos(\phi/2)-\sin(\phi/2)] \qquad \phi \in (\Psi-3\pi/2,-\pi/2]$$

These rather cumbersome equations can be written in a simplified form if we introduce the following notation ("<" refers to $\Psi \leq \pi/2$, while ">" refers to $\Psi > \pi/2$):

$$f_0(\phi) = 1$$

$$f_1(\phi) = \frac{\pi}{2}\sin(\Psi/2)$$

$$f_2(\phi) = 2\cos(\Psi/2)+\sin(\Psi/2) \qquad (C.39)$$

$$f_3(\phi) = \phi\sin(\Psi/2)$$

$$f_4(\phi) = \sqrt{2}\sin(\phi/2)$$

$$f_5(\phi) = \sqrt{2}\cos(\phi/2)$$

$$
\begin{aligned}
\alpha_0^< &= \alpha_0^> = \Phi-\pi \\
\alpha_1^< &= \alpha_2^> = \max[\Phi-\pi, \Psi-3\pi/2] \\
\alpha_2^< &= \alpha_1^> = \max[\Phi-\pi, -\Psi-\pi/2] \\
\alpha_3^< &= \alpha_3^> = \max[\Phi-\pi, -\pi/2] \\
\alpha_4^< &= \alpha_5^> = \max[\Phi-\pi, \Psi-\pi/2] \\
\alpha_5^< &= \alpha_4^> = \max[\Phi-\pi, -\Psi+\pi/2] \\
\alpha_6^< &= \alpha_6^> = \pi/2 \\
\alpha_7^< &= \alpha_8^> = \min[\Phi+\pi, \Psi+\pi/2] \\
\alpha_8^< &= \alpha_7^> = \min[\Phi+\pi, -\Psi+3\pi/2] \\
\alpha_9^< &= \alpha_9^> = \min[\Phi+\pi, 3\pi/2] \\
\alpha_{10}^< &= \alpha_{11}^> = \min[\Phi+\pi, \Psi+3\pi/2] \\
\alpha_{11}^< &= \alpha_{10}^> = \min[\Phi+\pi, -\Psi+5\pi/2] \\
\alpha_{12}^< &= \alpha_{12}^> = \Phi+\pi
\end{aligned}
\qquad (C.40)
$$

In addition, let $A_{ijp}^{\lessgtr}$ be defined as in table C-1.

With this notation (C.34), (C.35), (C.37), and (C.38) can be expressed as

Table C-1

Definition of $A^{\lessgtr}_{ijp}$

j	p	$\psi \lessgtr \pi/2$	i = 1	2	3	4	5	6	7	8	9	10	11	12
0	N	<	0	0	0	4	4	4	0	0	0	4	4	4
		>	0	0	0	4	4	4	0	0	0	4	4	4
	S	<	4	4	4	0	0	0	4	4	4	0	0	0
		>	4	4	4	0	0	0	4	4	4	0	0	0
1	N	<	5	2	1	1	2	1	1	2	5	5	2	-3
		>	5	4	1	1	0	1	1	4	5	5	0	-3
	S	<	-1	2	3	3	2	3	3	2	-1	-1	2	7
		>	-1	0	3	3	4	3	3	0	-1	-1	4	7
2	N	<	-1	0	-1	-1	-2	-1	-1	0	-1	-1	-2	-1
		>	-1	-2	-1	-1	0	-1	-1	-2	-1	-1	0	-1
	S	<	-1	-2	-1	-1	0	-1	-1	-2	-1	-1	0	-1
		>	-1	0	-1	-1	-2	-1	-1	0	-1	-1	-2	-1
3	N	<	1	0	-1	-1	0	1	1	0	-1	-1	0	1
		>	1	0	-1	-1	0	1	1	0	-1	-1	0	1
	S	<	-1	0	1	1	0	-1	-1	0	1	1	0	-1
		>	-1	0	1	1	0	-1	-1	0	1	1	0	-1
4	N	<	-1	0	1	-1	0	-1	1	0	-1	1	0	1
		>	-1	0	1	-1	-2	-1	1	0	-1	1	2	1
	S	<	1	0	-1	1	0	1	-1	0	1	-1	0	-1
		>	1	0	-1	1	2	1	-1	0	1	-1	-2	-1
5	N	<	-1	0	-1	1	0	-1	1	0	1	-1	0	1
		>	-1	-2	-1	1	0	-1	1	2	1	-1	0	1
	S	<	1	0	1	-1	0	1	-1	0	-1	1	0	-1
		>	1	2	1	-1	0	1	-1	-2	-1	1	0	-1

$$\frac{\upsilon^{\lesseqgtr}_{Op1}(\phi)}{U_m} = \sum_{j=0}^{5} A^{\lesseqgtr}_{ijp} f_j(\phi) \quad ; \quad \phi \in [\alpha^{\lesseqgtr}_{i-1}, \alpha^{\lesseqgtr}_{i}] \quad ;$$

$$i = 1,2,3 \quad ; \quad p = N,S \qquad (C.41)$$

The rest of the υ_{Opi} functions can be evaluated in a like manner, and comes as no surprise that they can all be combined and written as

$$\frac{\upsilon^{\lesseqgtr}_{Opk}(\phi)}{U_m} = \sum_{j=0}^{5} A^{\lesseqgtr}_{ijp} f_j(\phi) \quad ; \quad \phi \in [\alpha^{\lesseqgtr}_{i-1}, \alpha^{\lesseqgtr}_{i}] \quad ;$$

$$i = 3k-2,\ldots,3k \quad ; \quad p = N,S \quad ; \quad k = 1,\ldots,4 \qquad (C.42)$$

We can now combine (C.42) with (C.15) and (C.16) to give an expression for U_{Op}:

$$\frac{U^{\lesseqgtr}_{Op}(\Phi,\sigma)}{U_m} = \frac{1}{\sigma\sqrt{(2\pi)}} \sum_{i=1}^{12} \int_{\alpha^{\lesseqgtr}_{i-1}}^{\alpha^{\lesseqgtr}_{i}} d\phi \; e^{-(\phi-\Phi)^2/2\sigma^2} \sum_{j=0}^{5} A^{\lesseqgtr}_{ijp} f_j(\phi) \quad ; \quad p = N,S \qquad (C.43)$$

Using the integral definitions given in (C.25) through (C.30), we now have

$$\frac{U_{Op}^{\lessgtr}(\Phi,\sigma)}{U_m} = \sum_{i=1}^{12} \left\{ \left[\sum_{j=0}^{2} A_{ijp}^{\lessgtr} f_j(\phi) \right] I_0(\alpha_{i-1},\alpha_i) + A_{i3p}^{\lessgtr} \sin(\Psi/2) I_1(\alpha_{i-1},\alpha_i) \right.$$

$$\left. + \sqrt{2} A_{i4p}^{\lessgtr} I_c(\alpha_{i-1},\alpha_i) + \sqrt{2} A_{i5p}^{\lessgtr} I_s(\alpha_{i-1},\alpha_i) \right\} \quad ;$$

$$p = N,S \qquad (C.44)$$

Figure C-5 shows U_{ON}/U_m as a function of Φ for a range of values of σ and of V_{sw}/U_m. U_{OS}/U_m can be related to these curves by the relationship

$$U_{OS}(\Phi,\sigma) = U_{ON}(\pi-\Phi,\sigma) \qquad (C.45)$$

Assumption B -- see (C.10) and (C.11)

$V_{sw}/U_m \leq \pi$

In this case the forms of U_{ON} and U_{OS} are particularly simple; it can be shown that

$$\frac{U_{ON}}{U_m} = \frac{V_{sw}}{2\pi U_m} [\pi I_0(\Phi-\pi,\Phi+\pi) - I_{c2}(-\pi,\pi)]$$

$$\frac{U_{OS}}{U_m} = \frac{V_{sw}}{2\pi U_m} [\pi I_0(\Phi-\pi,\Phi+\pi) + I_{c2}(-\pi,\pi)] \qquad (C.46)$$

$V_{sw}/U_m > \pi$

The derivation of U_{ON} and U_{OS} in this case parallels that given in

Figure C-5

Resultant relative merging rates for open field lines at the northern polar neutral point for Assumption A. Note the changing vertical scale. Since

$$U_{ON}(\Phi,\sigma) = U_{OS}(\pi-\Phi,\sigma)$$

and

$$U_{ON}(\Phi,\sigma)+U_{OS}(\Phi,\sigma) = \min[V_{sw},4U_m]$$

we have

$$U_{ON}(\Phi,\sigma)+U_{OS}(\pi-\Phi,\sigma) = \min[V_{sw},4U_m]$$

and, as a consequence,

$$U_{ON}(\pi/2,\sigma) = \min[V_{sw}/2,2U_m]$$

In plotting U_{ON}/U_m, therefore, the vertical scales were chosen so as to reflect these symmetries. On all plots, the midpoint of the vertical scale corresponds to $V_{sw}/2U_m$, while the distance between each pair of tick marks on the vertical scale corresponds to $V_{sw}/10U_m$.

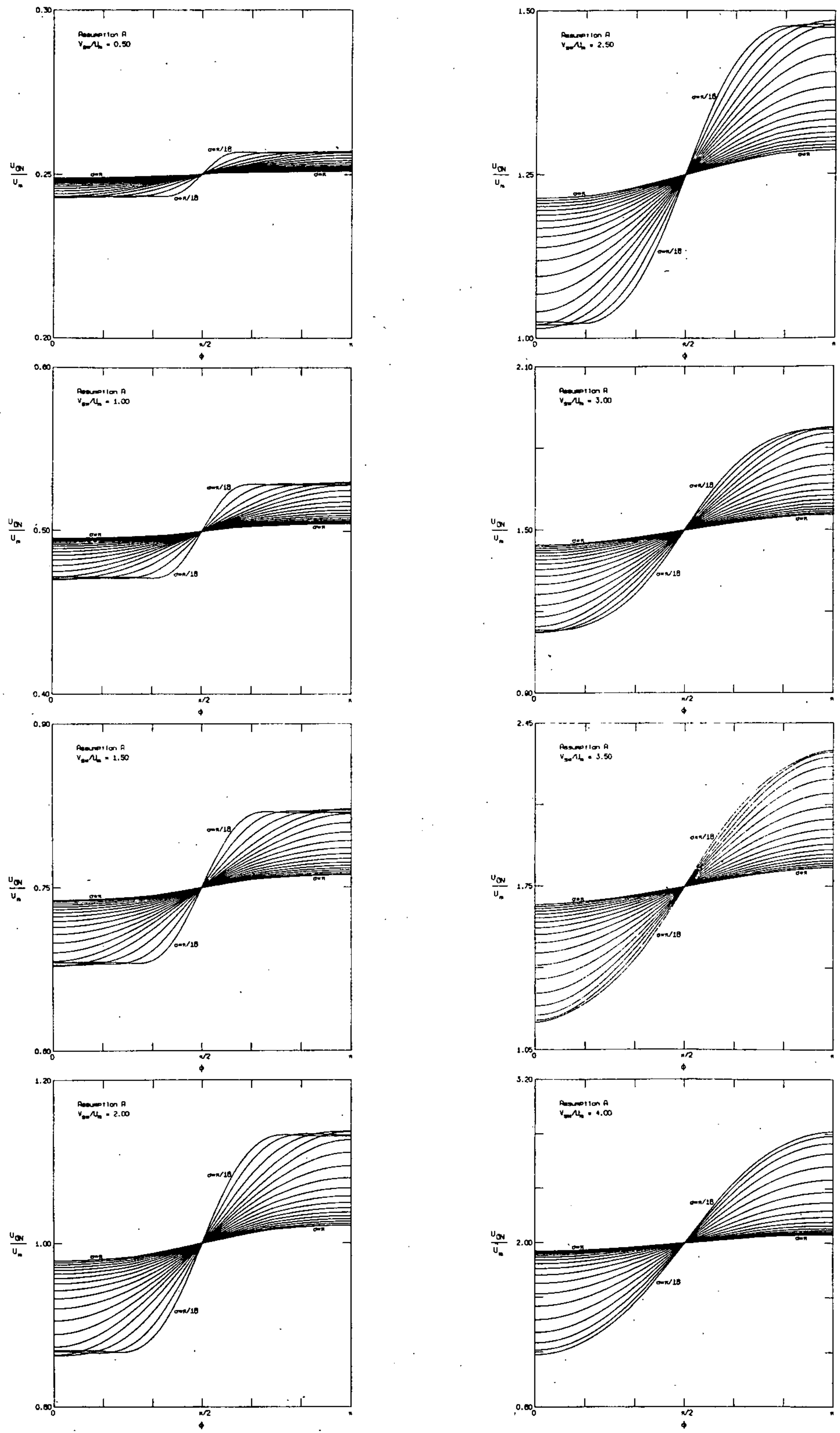
Assumption A
Assumption A
Assumption A
Assumption A
Assumption A
Assumption A
Assumption A
Assumption A
σ=π/18
σ=π
π/2
π
ϕ

detail for Assumption A to the extent that it is sufficient to merely specify the results of the derivation. In order to do so concisely, we will use the notation of (C.40) and define $g_j(\phi)$ as

$$\begin{aligned} g_0(\phi) &= V_{sw}/2U_m \\ g_1(\phi) &= \pi/[4\sin(\Psi/2)] \\ g_2(\phi) &= \phi/[2\sin(\Psi/2)] \\ g_3(\phi) &= \sqrt{2}\cos(\phi/2) \\ g_4(\phi) &= \sqrt{2}\sin(\phi/2) \\ g_5(\phi) &= \cos(\phi)/[2\sin(\Psi/2)] \end{aligned} \qquad (C.47)$$

With this notation and the definition of $B^{\lessgtr}_{ijp}$ given in table C-2, we have (as before, "<" refers to $\Psi \leq \pi/2$, while ">" refers to $\Psi > \pi/2$):

$$\frac{v^{\lessgtr}_{Opk}(\phi)}{U_m} = \sum_{j=0}^{5} B^{\lessgtr}_{ijp} g_j(\phi) \quad ; \quad \phi \in [\alpha^{\lessgtr}_{i-1}, \alpha^{\lessgtr}_{i}] \quad ;$$

$$i = 3k-2,\ldots,3k \quad ; \quad p = N,S \quad ; \quad k = 1,\ldots,4 \qquad (C.48)$$

which can be shown to yield

Table C-2

Definition of $B^{<}_{>ijp}$

j	p	ψ <> $\pi/2$	i = 1	2	3	4	5	6	7	8	9	10	11	12
0	N	<	1	0	1	1	2	1	1	0	1	1	2	1
		>	1	2	1	1	0	1	1	2	1	1	0	1
	S	<	1	2	1	1	0	1	1	2	1	1	0	1
		>	1	0	1	1	2	1	1	0	1	1	2	1
1	N	<	-3	0	1	1	0	1	1	0	-3	-3	0	5
		>	-3	-2	1	1	2	1	1	-2	-3	-3	2	5
	S	<	3	0	-1	-1	0	-1	-1	0	3	3	0	-5
		>	3	2	-1	-1	-2	-1	-1	2	3	3	-2	-5
2	N	<	-1	0	1	1	0	-1	-1	0	1	1	0	-1
		>	-1	0	1	1	0	-1	-1	0	1	1	0	-1
	S	<	1	0	-1	-1	0	1	1	0	-1	-1	0	1
		>	1	0	-1	-1	0	1	1	0	-1	-1	0	1
3	N	<	1	0	-1	-1	-2	-1	-1	0	1	1	2	1
		>	1	0	-1	-1	0	-1	-1	0	1	1	0	1
	S	<	-1	0	1	1	2	1	1	0	-1	-1	-2	-1
		>	-1	0	1	1	0	1	1	0	-1	-1	0	-1
4	N	<	-1	-2	-1	-1	0	1	1	2	1	1	0	-1
		>	-1	0	-1	-1	0	1	1	0	1	1	0	-1
	S	<	1	2	1	1	0	-1	-1	-2	-1	-1	0	1
		>	1	0	1	1	0	-1	-1	0	-1	-1	0	1
5	N	<	-1	0	-1	-1	0	-1	-1	0	-1	-1	0	-1
		>	-1	-2	-1	-1	-2	-1	-1	-2	-1	-1	-2	-1
	S	<	1	0	1	1	0	1	1	0	1	1	0	1
		>	1	2	1	1	2	1	1	2	1	1	2	1

$$\frac{U^{\lessgtr}_{0p}(\Phi,\sigma)}{U_m} = \sum_{i=1}^{12}\Big\{[B^{\lessgtr}_{i0p}g_0(\phi)+B^{\lessgtr}_{i1p}g_1(\phi)]I_0(\alpha_{i-1},\alpha_i)$$

$$+ \tfrac{1}{2}B_{i2p}I_1(\alpha_{i-1},\alpha_i) + \sqrt{2}B_{i3p}I_c(\alpha_{i-1},\alpha_i)$$

$$+ \sqrt{2}B^{\lessgtr}_{i4p}I_s(\alpha_{i-1},\alpha_i) + \tfrac{1}{2}B^{\lessgtr}_{i5p}I_{c2}(\alpha_{i-1},\alpha_i)\Big\} \quad ;$$

$$p = N,S \qquad (C.49)$$

Figure C-6 shows U_{ON}/U_m (and, hence, U_{OS}/U_m [*cf.* (C.45)]) as a function of Φ for a range of values of σ and of V_{sw}/U_m.

Assumption C -- see (C.12) and (C.13)

Here again the derivation of U_{ON} and U_{OS} parallels that for Assumption A closely, and we will once again define a convenient notation:

$$h_0(\phi) = 2\cos(\Psi/2)$$

$$h_1(\phi) = \sqrt{2}\cos(\phi/2) \qquad (C.50)$$

$$h_2(\phi) = \sqrt{2}\sin(\phi/2)$$

and we will let $C^{\lessgtr}_{ijp}$ be defined as in table C-3. Then the resultant expression for U_{0p} can be written as

Figure C-6

Resultant relative merging rates for open field lines at the northern polar neutral point for Assumption B. The vertical scale convention specified in the caption for figure C-5 is observed here as well.

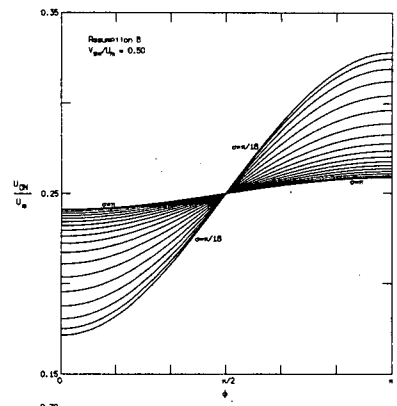
Assumption B
$V_{gw}/U_{\infty} = 0.50$
$\omega = \pi/16$
$\omega = \pi$
$\frac{U_{ON}}{U_{\infty}}$
ϕ

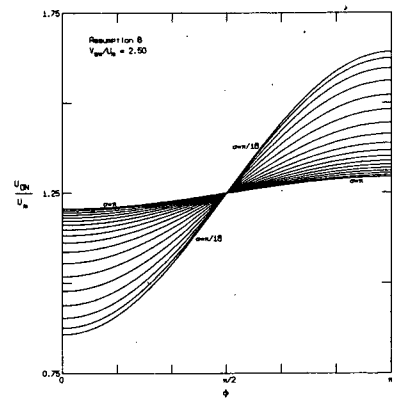
Assumption B
$V_{gw}/U_{\infty} = 2.50$
$\omega = \pi/16$
$\omega = \pi$
$\frac{U_{ON}}{U_{\infty}}$
ϕ

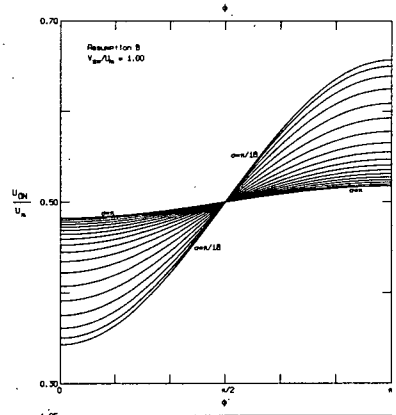
Assumption B
$V_{gw}/U_{\infty} = 1.00$
$\omega = \pi/16$
$\omega = \pi$
$\frac{U_{ON}}{U_{\infty}}$
ϕ

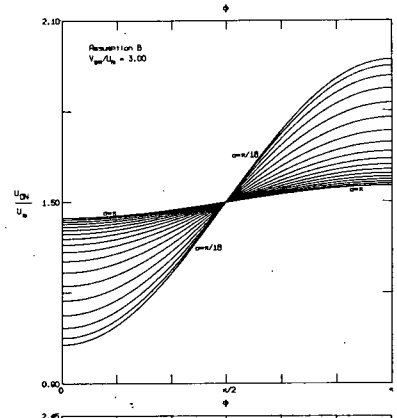
Assumption B
$V_{gw}/U_{\infty} = 3.00$
$\omega = \pi/16$
$\omega = \pi$
$\frac{U_{ON}}{U_{\infty}}$
ϕ

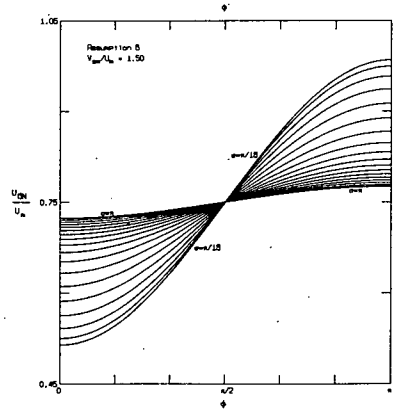
Assumption B
$V_{gw}/U_{\infty} = 1.50$
$\omega = \pi/16$
$\omega = \pi$
$\frac{U_{ON}}{U_{\infty}}$
ϕ

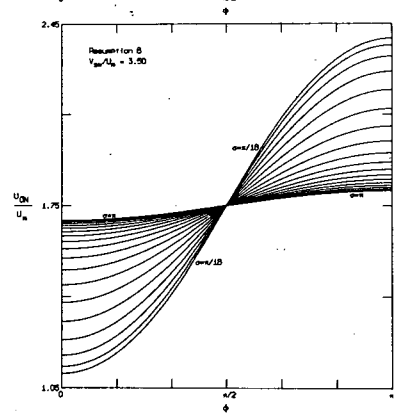
Assumption B
$V_{gw}/U_{\infty} = 3.50$
$\omega = \pi/16$
$\omega = \pi$
$\frac{U_{ON}}{U_{\infty}}$
ϕ

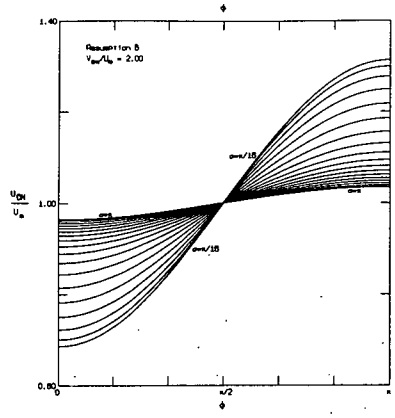
Assumption B
$V_{gw}/U_{\infty} = 2.00$
$\omega = \pi/16$
$\omega = \pi$
$\frac{U_{ON}}{U_{\infty}}$
ϕ

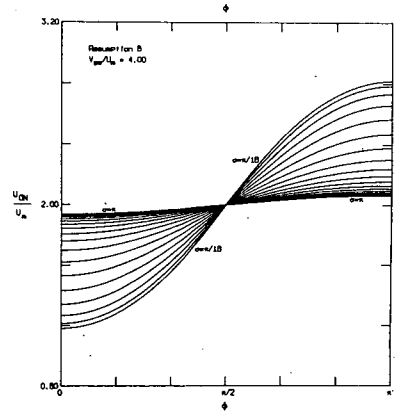
Assumption B
$V_{gw}/U_{\infty} = 4.00$
$\omega = \pi/16$
$\omega = \pi$
$\frac{U_{ON}}{U_{\infty}}$
ϕ

Table C-3

Definition of $C^{<}_{ijp}$

j	p	$\Psi \lessgtr \pi/2$	i = 1	2	3	4	5	6	7	8	9	10	11	12
0	N	<	1	0	1	1	2	1	1	0	1	1	2	1
		>	1	2	1	1	0	1	1	2	1	1	0	1
	S	<	1	2	1	1	0	1	1	2	1	1	0	1
		>	1	0	1	1	2	1	1	0	1	1	2	1
1	N	<	1	0	-1	-1	-2	-1	-1	0	1	1	2	1
		>	1	0	-1	-1	0	-1	-1	0	1	1	0	1
	S	<	-1	0	1	1	2	1	1	0	-1	-1	-2	-1
		>	-1	0	1	1	0	1	1	0	-1	-1	0	-1
2	N	<	-1	-2	-1	-1	0	1	1	2	1	1	0	-1
		>	-1	0	-1	-1	0	1	1	0	1	1	0	-1
	S	<	1	2	1	1	0	-1	-1	-2	-1	-1	0	1
		>	1	0	1	1	0	-1	-1	0	-1	-1	0	1

$$\frac{U_{0p}^{\gtrless}(\Phi,\sigma)}{U_m} = \sum_{i=1}^{12}\left\{C_{i0p}^{\gtrless} h_0(\phi) I_0(\alpha_{i-1},\alpha_i) + \sqrt{2}C_{i1p}^{\gtrless} I_c(\alpha_{i-1},\alpha_i) + \sqrt{2}C_{i2p}^{\gtrless} I_s(\alpha_{i-1},\alpha_i)\right\} \quad ; \quad p = N,S \qquad (C.51)$$

U_{0N}/U_m, as given by (C.51), is shown in figure C-7.

Results

Since the uncertainty concerning the proper value of U_m and the interplanetary plasma and magnetic field parameters at the polar neutral points prevents the determination of *absolute* merging rates, the purpose of this study is to determine whether the *relative* merging rates for open field lines at the two poles is sufficient to yield the relative access window locations observed with the OGO-4 data. Results from the EDP observations (see Sections VII and VIII) indicate that the ratio between the position of the β-high polar latitude access window to the position of the α-high polar latitude access window is typically ∿5:1 (∿1500 $R_\oplus$: ∿300 $R_\oplus$ behind the earth). For this field configuration, this ratio would necessitate a similar ratio between the length of the β-geomagnetic tail and the length of the α-geomagnetic tail. This could be accomplished if the ratio of α-pole open field merging rate to β-pole open field merging rate were comparable to 5:1.

Figures C-8 to C-10 show the north to south open field line merging rate ratio for each of the three assumptions and for a range of

Figure C-7

Resultant relative merging rates for open field lines at the northern polar neutral point for Assumption C. The vertical scale convention specified in the caption for figure C-6 is observed here as well.

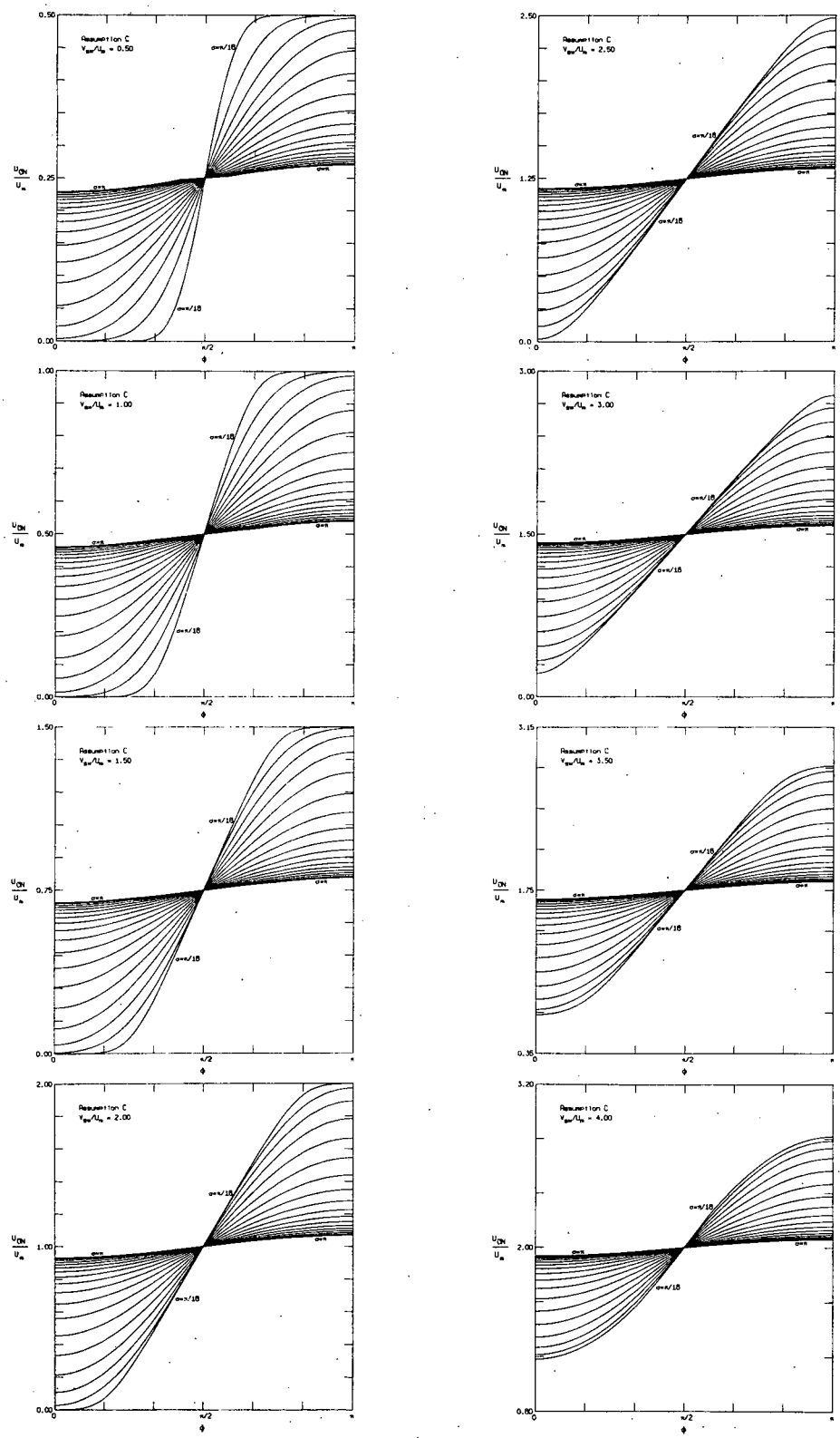
Respuesta C
V_{gs}/U_{in} = 0.50
V_{gs}/U_{in} = 2.50
V_{gs}/U_{in} = 1.00
V_{gs}/U_{in} = 3.00
V_{gs}/U_{in} = 1.50
V_{gs}/U_{in} = 3.50
V_{gs}/U_{in} = 2.00
V_{gs}/U_{in} = 4.00
$\frac{U_{ON}}{U_{in}}$
ϕ
0
π/2
π

Figure C-8

Ratio between the open field line merging rates at the northern and southern polar neutral points for Assumption A.

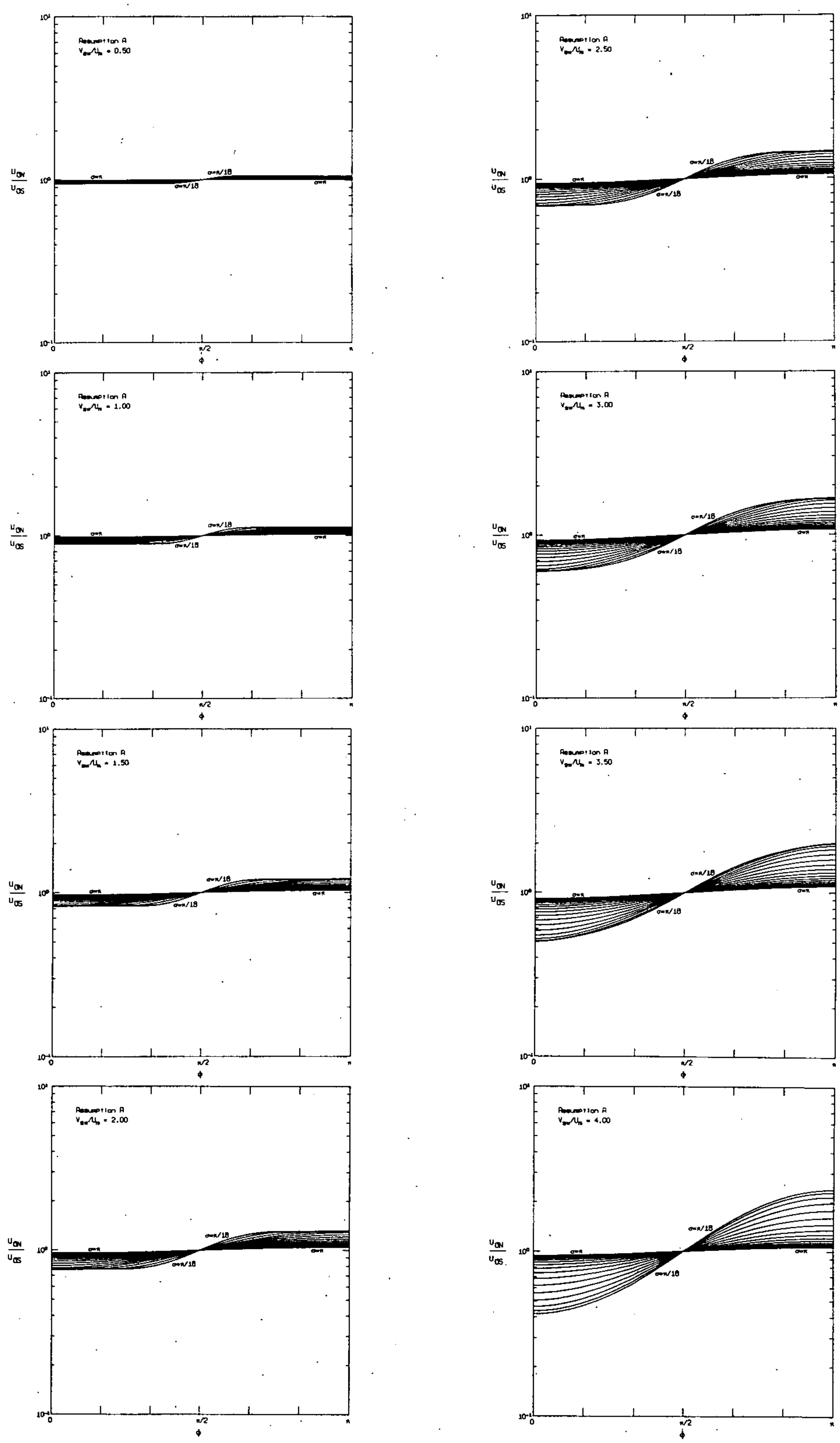
Assumption A
Assumption A
Assumption A
Assumption A
Assumption A
Assumption A
Assumption A
Assumption A
σ=π/18
σ=π
π/2
φ

Figure C-9

Ratio between open field line merging rates at the northern and southern polar neutral points for Assumption B.

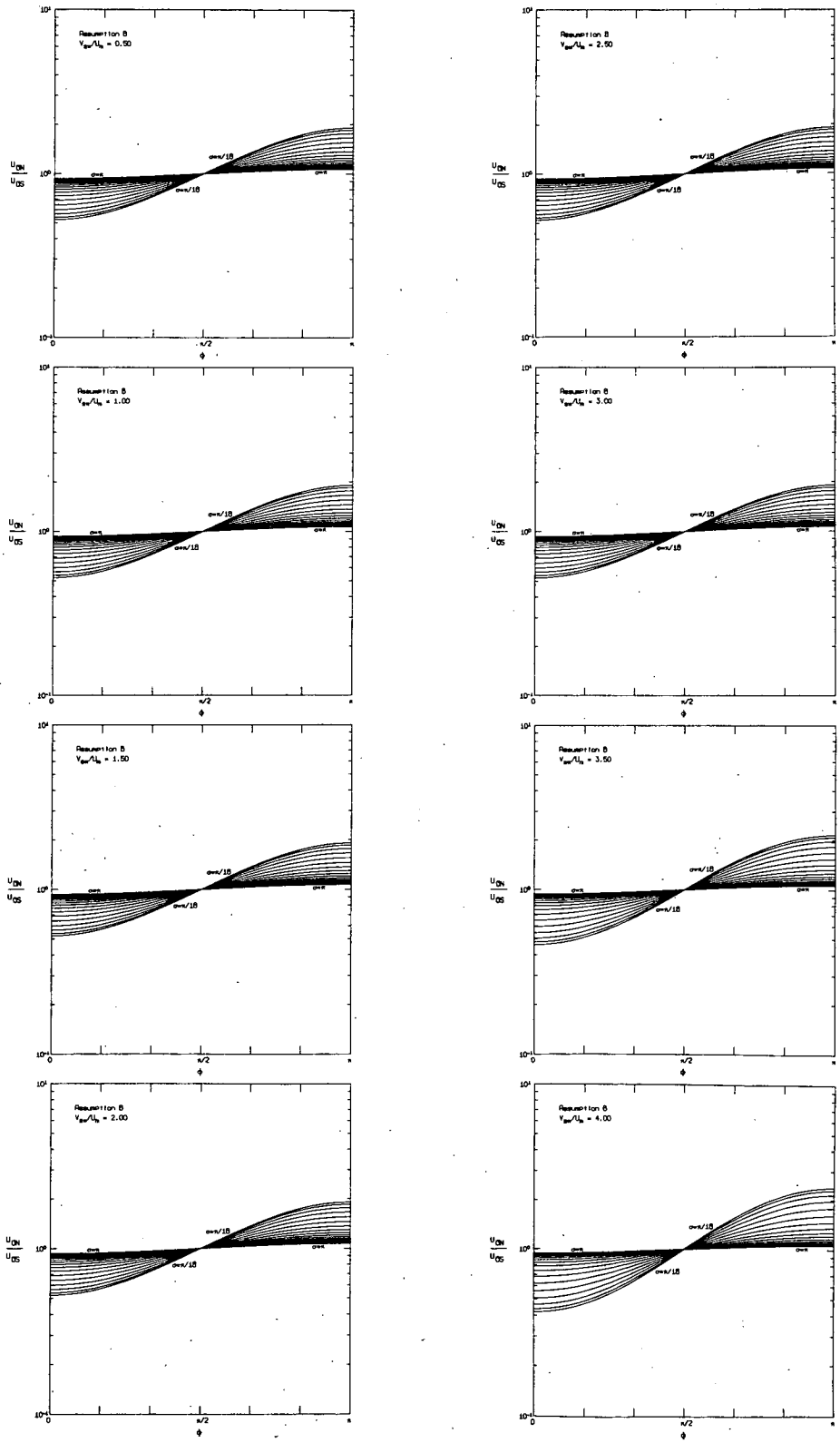
Resurrection B
V_{sw}/U_{∞} = 0.50
Resurrection B
V_{sw}/U_{∞} = 2.50
Resurrection B
V_{sw}/U_{∞} = 1.00
Resurrection B
V_{sw}/U_{∞} = 3.00
Resurrection B
V_{sw}/U_{∞} = 1.50
Resurrection B
V_{sw}/U_{∞} = 3.50
Resurrection B
V_{sw}/U_{∞} = 2.00
Resurrection B
V_{sw}/U_{∞} = 4.00
$\frac{U_{ON}}{U_{OS}}$
ϕ
0
π/2
π

Figure C-10

Ratio between open field line merging rates at the northern and southern polar neutral points for Assumption C. Note the change in vertical scale between the sixth and seventh graphs (i.e., between $V_{sw}/U_m = 3.00$ and $V_{sw}/U_m = 3.50$).

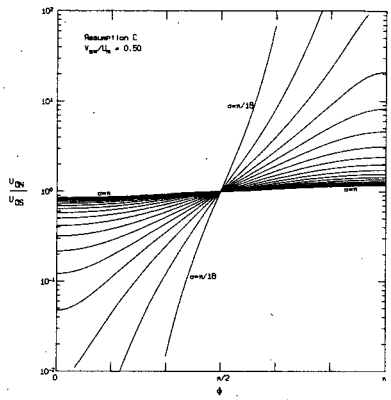
Resumption C
V_{sw}/U_{ts} = 0.50
α=π/18
α=π
$\frac{U_{GN}}{U_{OS}}$
φ

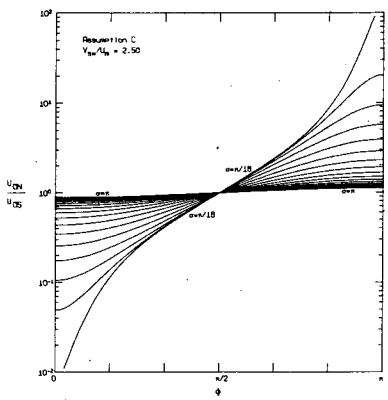
Resumption C
V_{sw}/U_{ts} = 2.50
α=π/18
α=π
$\frac{U_{GN}}{U_{OS}}$
φ

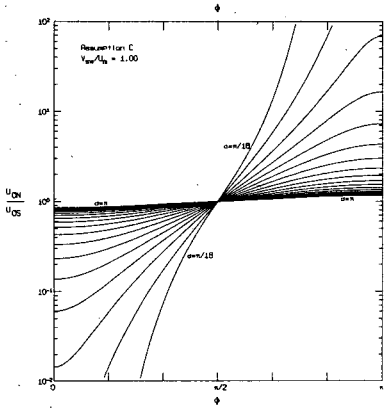
Resumption C
V_{sw}/U_{ts} = 1.00
α=π/18
α=π
$\frac{U_{GN}}{U_{OS}}$
φ

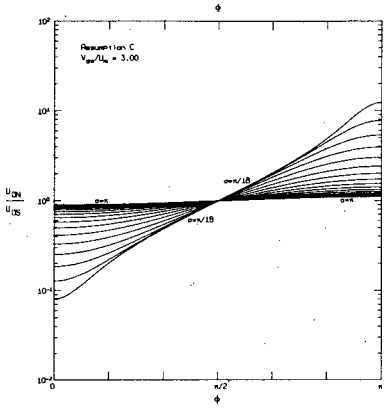
Resumption C
V_{sw}/U_{ts} = 3.00
α=π/18
α=π
$\frac{U_{GN}}{U_{OS}}$
φ

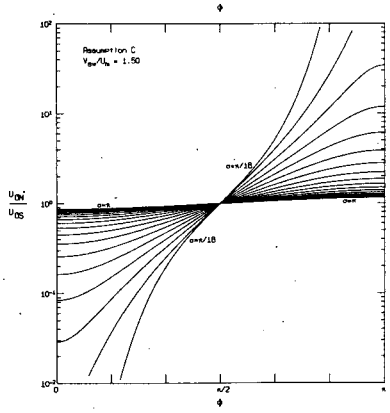
Resumption C
V_{sw}/U_{ts} = 1.50
α=π/18
α=π
$\frac{U_{GN}}{U_{OS}}$
φ

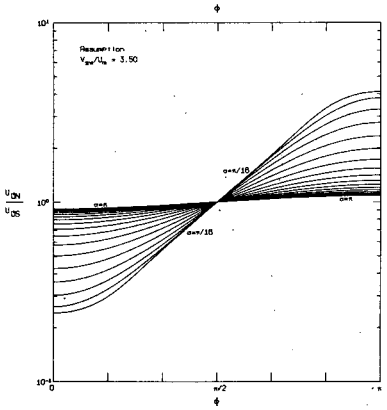
Resumption
V_{sw}/U_{ts} = 3.50
α=π/18
α=π
$\frac{U_{GN}}{U_{OS}}$
φ

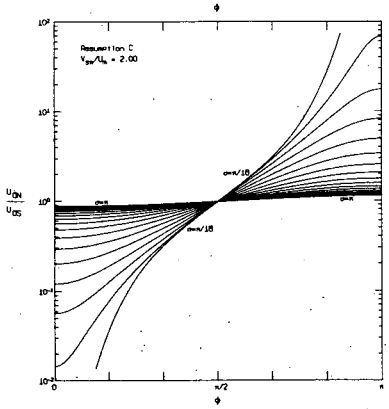
Resumption C
V_{sw}/U_{ts} = 2.00
α=π/18
α=π
$\frac{U_{GN}}{U_{OS}}$
φ

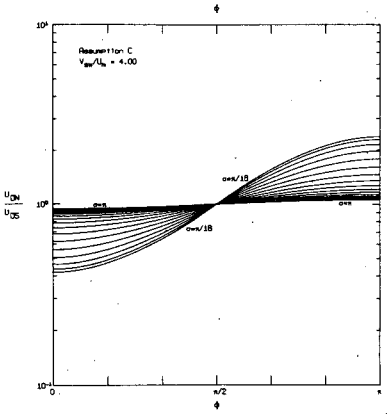
Resumption C
V_{sw}/U_{ts} = 4.00
α=π/18
α=π
$\frac{U_{GN}}{U_{OS}}$
φ

values of σ and of V_{sw}/U_m. Note that for values of V_{sw}/U_m greater than 4.0 these ratios will not change. These figures indicate that a 5:1 ratio between the open field merging rates at the two poles is possible only with Assumption C. The maximum value of U_{ON}/V_{OS} shown is 2.38 for Assumptions A and B ($\Phi=\pi$, $\sigma=\pi/18$, $V_{sw}/U_m=4.0$). Figure C-11 indicates the range of parameters which will give $U_{ON}/U_{OS} \geq 5$ for Assumption C.

These results are discussed further in Section VII.

Figure C-11

Contours of U_{ON}/U_{OS} = 5.0 in Φ-(V_{sw}/U_m) space for Assumption C. The range of Φ and V_{sw}/U_m corresponding to U_{ON}/U_{OS} > 5 for a given value of σ is represented by that region below and to the right of the appropriate contour.

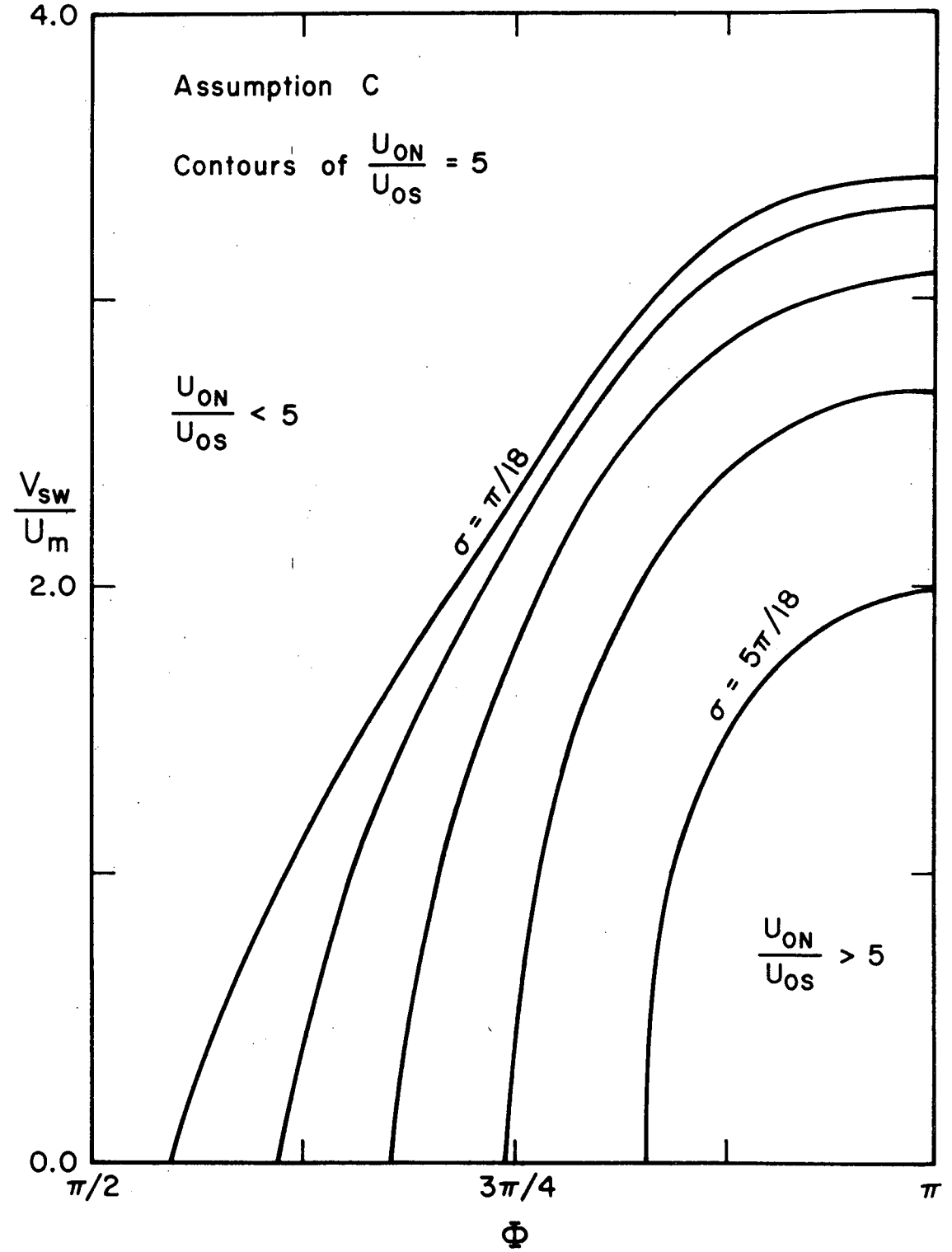
4.0
Assumption C
Contours of $\frac{U_{ON}}{U_{os}} = 5$
$\frac{U_{ON}}{U_{os}} < 5$
$\sigma = \pi/18$
$\sigma = 5\pi/18$
$\frac{U_{ON}}{U_{os}} > 5$
$\frac{V_{sw}}{U_m}$
2.0
0.0
$\pi/2$
$3\pi/4$
π
Φ

REFERENCES

1. L. J. Cahill, Jr., "Preliminary Results of Magnetic Field Measurements in the Tail of the Geomagnetic Cavity," *Transactions of the American Geophysical Union, 45* (1964), 231.

2. J. W. Dungey, "Interplanetary Magnetic Field and the Auroral Zones," *Physical Review Letters, 6* (1961), 47.

3. A. J. Dessler, "The Length of the Magnetospheric Tail," *Journal of Geophysical Research, 69* (1964), 3913.

4. L. A. Frank, "Comments on a Proposed Magnetospheric Model," *Journal of Geophysical Research, 76* (1971), 2512.

5. H. E. Petschek, "Magnetic Field Annihilation," in *AAS-NASA Symposium on the Physics of Solar Flares*, ed. by W. N. Hess, NASA SP-50 (1964), 425.

6. P. A. Sturrock, "Explosions in Galaxies and Quasars," in *Plasma Instabilities in Astrophysics; Proceedings of the Conference, Monterey, California, October 14-17, 1968*, D. G. Wentzel and D. A. Tidman, eds., Gordon and Breach, Science Publishers, Inc., New York, 1969, p. 297.

7. J. A. Van Allen, "Energetic Particle Phenomena in the Earth's Magnetospheric Tail," in *Particles and Fields in the Magnetosphere; Summer Advanced Study Institute, Symposium, University*

of California, Santa Barbara, California, August 4-15, 1969, B. M. McCormac, ed., Dordrecht, D. Reidel Publishing Co., 1970, p. 111.

8. J. A. Van Allen, "On the Electric Field in the Earth's Distant Magnetotail," *Journal of Geophysical Research, 75* (1970), 29.

9. K. A. Anderson and R. P. Lin, "Observation of Interplanetary Field Lines in the Magnetotail," *Journal of Geophysical Research, 74* (1969), 3953.

10. F. C. Michel and A. J. Dessler, "Diffusive Entry of Solar-flare Particles into Geomagnetic Tail," *Journal of Geophysical Research, 75* (1970), 6061.

11. L. C. Evans and E. C. Stone, "Access of Solar Protons into the Polar Cap -- A Persistent North-South Asymmetry," *Journal of Geophysical Research, 74* (1969), 5127.

12. Y. Hakura, "Entry of Solar Cosmic Rays Into the Polar Cap Atmosphere," *Journal of Geophysical Research, 72* (1967), 1461.

13. G. C. Reid and H. H. Sauer, "Evidence for Non uniformity of Solar-proton Precipitation over the Polar Caps," *Journal of Geophysical Research, 72* (1967), 4383.

14. C. O. Bostrom, J. W. Kohl, and D. J. Williams, "The February 5, 1965, Solar Proton Event, I," *Journal of Geophysical Research, 72* (1967), 4487.

15. D. J. Williams and C. O. Bostrom, "The February 5, 1965, Solar Proton Event, II," *Journal of Geophysical Research, 72* (1967),

4497.

16. J. B. Blake, G. A. Paulikas, and S. C. Freden, "Latitude-intensity Structure and Pitch-angle Distributions of Low-energy Solar Cosmic Rays at Low Altitude," *Journal of Geophysical Research, 73* (1968), 4927.

17. S. M. Krimigis, J. A. Van Allen, and T. P. Armstrong, "Solar Particle Observations inside the Magnetosphere during the 7 July 1966 Proton Flare Event," in *The Proton Flare Project (The July 1966 Event)*, A. C. Stickland, ed., Massachusetts Institute of Technology Press, Cambridge, Mass, 1969, p. 395.

18. J. R. Burrows, I. B. McDiarmid, and M. D. Wilson, "On the High Latitude Limit of Closed Geomagnetic Field Lines," *Proceedings of the IEEE, 57* (1969), 1051.

19. D. J. Williams and C. O. Bostrom, "Proton Entry into the Magnetosphere on May 26, 1967," *Journal of Geophysical Research, 74* (1969), 3019.

20. R. D. Sharp, D. L. Carr, and R. G. Johnson, "Satellite Observations of the Average Properties of Auroral Particle Precipitation: Latitudinal Variations," *Journal of Geophysical Research, 74* (1969), 4618.

21. C. O. Bostrom, "Entry of Low Energy Solar Protons into the Magnetosphere," in *Intercorrelated Satellite Observations Related to Solar Events; European Space Research Organization, Annual ESLAB/ESRIN, Symposium, 3rd, Noordwijk, Netherlands,*

September 16-19, 1969, Proceedings, V. Manno and D. E. Page, eds., Dordrecht, D. Reidel Publishing Co., 1970, p. 229ff.

22. I. B. McDiarmid and J. R. Burrows, "Relation of Solar Proton Latitude Profiles to Outer Radiation Zone Electron Measurements," *Journal of Geophysical Research, 74* (1969), 6239.

23. G. A. Paulikas, J. B. Blake, and A. L. Vampola, "Solar Particle Observations over the Polar Caps," in *Particles and Fields in the Magnetosphere; Summer Advanced Study Institute, Symposium, University of California, Santa Barbara, California, August 4-15, 1969, Proceedings*, B. M. McCormac, ed., D. Reidel Publishing Co., Dordrecht, 1970, p. 141ff.

24. J. Englemann, R. J. Hynds, G. Morfill, F. Axisa, A. Bewick, A. C. Durney, and L. Koch, "Penetration of Solar Protons over the Polar Caps during the February 25th 1969 Event," *Journal of Geophysical Research, 76* (1971), 4245.

25. J. A. Van Allen, J. F. Fennell, and N. F. Ness, "Asymmetric Access of Energetic Solar Protons to the Earth's North and South Polar Caps," *Journal of Geophysical Research, 76* (1971), 4262.

26. G. E. Morfill and J. J. Quenby, "The Entry of Solar Protons over the Polar Caps," to be published.

27. A. L. Vampola, "Access of Solar Electrons to Closed Field Lines," *Journal of Geophysical Research, 76* (1971), 36.

28. L. C. Evans, J. L. Fanselow, and E. C. Stone, "User's Notes

for Experiments C-08 and D-08 Rate Plots," Space Radiation Laboratory Internal Report No. 11, January, 1970.

29. W. E. Althouse, E. C. Stone, R. E. Vogt, and T. H. Harrington, "A Solar and Galactic Cosmic Ray Satellite Experiment," *IEEE Transactions on Nuclear Science, 15* (1967), 229.

30. J. F. Janni, *Calculations of Energy Loss, Range, Pathlength, Straggling, etc.*, Technical Report AFWL-TR-65-150, 1966.

31. L. C. Evans and E. C. Stone, "OGO-4, Experiment 08, Calibrations," Space Radiation Laboratory Internal Report No. 27, August, 1971.

32. J. E. Lupton and J. W. Brown, private communication, 1971.

33. J. E. Lupton, private communication, 1971.

34. OGO Experiment Bulletin F-143, "OGO Operations Summary Report June, 1969," Report No. 08672-6032-TO-00 (1969), 5.

35. L. C. Evans, "OGO-4 Data Coverage Plots," Space Radiation Laboratory Internal Report No. 25, August, 1971.

36. W. N. Hess, *The Radiation Belt and Magnetosphere*, Blaisdell Publishing Co., Division of Ginn and Co., Waltham, Mass., 1968, p. 57ff.

37. T. A. Fritz and D. A. Gurnett, "Diurnal and Latitudinal Effects Observed for 10 keV Electrons at Low Satellite Altitudes," *Journal of Geophysical Research, 70* (1965), 2485.

38. Cain, *et al.*, *Computation of the Main Geomagnetic Field from*

Spherical Harmonic Expansions, NSSDC 68-11, Goddard Space Flight Center, Greenbelt, Md., 1968.

39. E. A. Aguilar, J. L. Fanselow, and L. C. Evans, "Magnetic Tape Formats for Experiment 08 on OGO II and IV," Space Radiation Laboratory Internal Report No. 22.

40. I. B. McDiarmid and J. R. Burrows, "Latitude Profiles of Low-energy Solar Electrons, *Journal of Geophysical Research, 75* (1970), 3910.

41. H. I. West, Jr. and A. L. Vampola, "Simultaneous Observations of Solar Flare Electron Spectra in Interplanetary Space and within the Earth's Magnetosphere," *Physical Review Letters, 26* (1971), 458.

42. D. A. Bryant, T. L. Cline, U. D. Desai, and F. B. McDonald, "Studies of Solar Protons with Explorers XII and XIV," *Astrophysical Journal, 141* (1965), 478.

43. D. A. Bryant, T. L. Cline, U. D. Desai, and F. B. McDonald, "Continual Acceleration of Solar Protons in the MeV Range," *Physical Review Letters, 14* (1965), 481.

44. U. R. Rao, K. G. McCracken, and R. P. Bukata, "Cosmic-Ray Propagation Processes, II," *Journal of Geophysical Research, 72* (1967), 4325.

45. R. P. Lin and K. A. Anderson, "Electrons >40 keV and Protons >500 keV of Solar Origin," *Solar Physics, 1* (1967), 446.

46. C. Y. Fan, M. Pick, R. Pyle, J. A. Simpson, and D. R. Smith, "Protons Associated with Centers of Solar Activity and Their Propagation in Interplanetary Magnetic Field Regions Corotating with the Sun," *Journal of Geophysical Research, 73* (1968), 1555.

47. K. A. Anderson, "Electrons and Protons in Long Lived Streams of Energetic Particles," *Solar Physics, 6* (1969), 111.

48. J. F. Steljes, *Cosmic Ray NM-64 Neutron Monitor Data*, Atomic Energy of Canada Limited, AECL-3064, 1968.

49. J. A. Simpson, private communication, 1971.

50. R. P. Lin, S. W. Kahler, and E. C. Roelof, "Solar Flare Injection and Propagation of Low-energy Protons and Electrons in the Event of 7-9 July, 1966," *Solar Physics, 4* (1968), 338.

51. E. C. Stone, "Time Dependence of Non-Störmer cutoff for 1.5 MeV Protons in Quiet Geomagnetic Field," *Journal of Geophysical Research, 69* (1964), 3577.

52. E. N. Parker, "Dynamics of the Interplanetary Gas and Magnetic Field," *Astrophysical Journal, 128* (1958), 664.

53. D. H. Fairfield, "The Ordered Magnetic Field of the Magnetosheath," *Journal of Geophysical Research, 72* (1967), 5865.

54. N. F. Ness, C. S. Scearce, and J. B. Seek, "Initial Results of the IMP 1 Magnetic Field Experiment," *Journal of Geophysical Research, 69* (1964), 3531.

55. P. J. Coleman, Jr., "Variations in the Interplanetary Magnetic Field -- Mariner 2, I," *Journal of Geophysical Research, 71* (1966), 5509.

56. J. M. Wilcox and N. F. Ness, "Quasi-stationary Corotating Structure in the Interplanetary Medium," *Journal of Geophysical Research, 70* (1965), 5793.

57. J. M. Wilcox and D. S. Colburn, "Interplanetary Sector Structure in the Rising Portion of the Sunspot Cycle," *Journal of Geophysical Research, 74* (1969), 2388.

58. J. M. Wilcox and D. S. Colburn, "Interplanetary Sector Structure near the Maximum of the Sunspot Cycle," NASA-CR-110861; AD-707748, 1970.

59. K. G. McCraken and U. R. Rao, "Solar Cosmic Ray Phenomena," *Space Science Reviews, 11* (1970), 155.

60. J. J. O'Gallagher, "The Heliocentric Longitude Intensity Profile of 15-MeV Protons from the February 5, 1965, Solar Flare," *Journal of Geophysical Resaerch, 75* (1970), 1163.

61. M. A. Forman, "Convection-Dominated Transport of Solar Cosmic Rays," *Journal of Geophysical Research, 74* (1971), 759.

62. D. A. Bryant, T. L. Cline, U. D. Desai, and F. B. McDonald, "Explorer 12 Observations of Solar Cosmic Rays and Energetic Storm Particles after the Solar Flare of September 28, 1961," *Journal of Geophysical Research, 67* (1962), 4983.

63. K. G. McCracken, U. R. Rao, and N. F. Ness, "Interrelationship

of Cosmic-ray Anisotropies and the Interplanetary Magnetic Field," *Journal of Geophysical Research, 73* (1968), 4159.

64. U. R. Rao, F. R. Allum, W. C. Bartley, R. A. R. Palmeira, J. A. Harries, and K. G. McCracken, "Measurement of Cosmic Ray Anisotropy of Solar Origin by Explorer 34 Satellite," in *Solar Flares and Space Research; COSPAR, Plenary Meeting, 11th, Symposium, Tokyo, Japan, May 9-11, 1968, Proceedings*, C. de Jager and Z. Švestka, eds., North Holland Publishing Co., Amsterdam, 1969, p. 267ff.

65. K. G. McCracken, U. R. Rao, R. P. Bukata, and E. P. Keath, "The Decay Phase of Solar Flare Events," *Solar Physics, 18* (1971), 100.

66. K. G. McCracken, U. R. Rao, and R. P. Bukata, "Cosmic Ray Propagation Processes, 1, A study of the Cosmic-Ray Flare Effect," *Journal of Geophysical Research, 72* (1967), 4293.

67. E. N. Parker, "Interaction of the Solar Wind with the Geomagnetic Field," *Physics of Fluids, 1* (1958), 171.

68. D. B. Beard, "The Interaction of the Terrestrial Magnetic Field with the Solar Corpuscular Radiation," *Journal of Geophysical Research, 65* (1960), 3559.

69. J. R. Spreiter and B. R. Briggs, "Theoretical Determination of the Form of the Boundary of the Solar Corpuscular Stream Produced by the Interaction with the Magnetic Dipole Field of the Earth," *Journal of Geophysical Research, 67* (1962), 37.

70. J. R. Midgley and L. Davis, "Calculation by a Moment Technique of the Perturbation of the Geomagnetic Field by the Solar Wind," *Journal of Geophysical Research, 68* (1963), 5111.

71. W. N. Hess, *op. cit.*, p. 293ff.

72. D. H. Fairfield, "The Magnetic Field of the Magnetosphere and Tail," NASA-TM-X-63508; X-616-69-124, 1969.

73. D. H. Fairfield, "The Configuration of the Geomagnetic Field," NASA-TM-X-63891;X-692-70-163, 1970.

74. N. F. Ness, "The Earth's Magnetic Tail," *Journal of Geophysical Research, 70* (1965), 2989.

75. N. F. Ness, K. W. Behannon, C. S. Scearce, and S. C. Cantarano, "Observations of the Earth's Magnetic Tail and Neutral Sheet at 510,000 Kilometers by Explorer 33," *Journal of Geophysical Research, 72* (1967), 927.

76. N. F. Ness, "The Geomagnetic Tail," *United States National Academy of Sciences and NASA Goddard Space Flight Center, International Symposium on the Physics of the Magnetosphere, Washington, D. C., September 3-13, 1968, Reviews of Geophysics, 7* (1969), 97.

77. F. Mariani and N. F. Ness, "Observations of the Geomagnetic Tail at 500 Earth Radii by Pioneer 8," *Journal of Geophysical Research, 74* (1969), 5633.

78. G. L. Siscoe, F. L. Scarf, D. S. Intriligator, J. H. Wolfe, J. H. Binsack, H. S. Bridge, and V. M. Vasyliunas, "Evidence

for a Geomagnetic Wake at 500 Earth Radii," *Journal of Geophysical Research, 75* (1970), 5319.

79. N. F. Ness, C. S. Scearce, and S. C. Cantarano, "Probable Observation of the Geomagnetic Tail at 10^3 Earth Radii by Pioneer 7," *Journal of Geophysical Research, 72* (1967), 3769.

80. D. H. Fairfield, "Simultaneous Measurements on Three Satellites and the Observation of the Geomagnetic Tail at 1000 R_E," *Journal of Geophysical Research, 73* (1968), 6179.

81. D. S. Intriligator, J. H. Wolfe, D. D. McKibbin, and H. R. Collard, "Preliminary Comparison of Solar Wind Plasma Observations in the Geomagnetospheric Wake at 1000 and 500 Earth Radii," *Planetary and Space Science, 17* (1969), 321.

82. R. Gall, J. Jiménez, and L. Camacho, "Arrival of Low-energy Cosmic Rays *via* the Magnetospheric Tail," *Journal of Geophysical Research, 73* (1968), 1593.

83. R. Gall, J. Jiménez, and A. Orozco, "Direction of Approach of Cosmic Rays for High Latitude Stations," *Journal of Geophysical Research, 74* (1969), 3529.

84. P. A. Sweet, Proceedings of the International Astronomical Union Symposium on Electromagnetic Phenomena in Cosmical Physics, No. 6 (Stockholm, 1956), p. 123 (1958), *Nuovo Cimento,* Supplement 8, Section X (1958), 188.

85. E. N. Parker, "The Solar Flare Phenomena and the Theory of Reconnection and Annihilation of Magnetic Fields," *Astrophysical Journal, Supplement Series 77, 8* (1963), 177.

86. H. E. Petschek, "Reconnection and Annihilation of Magnetic Fields," in *The Solar Wind; Proceedings of a Conference, California Institute of Technology, Pasadena, California, April 1-4, 1964*, R. J. Mackin, Jr. and M. Neugebauer, eds., Jet Propulsion Laboratory, Pasadena, California, 1966, p. 221ff.

87. B. U. Ö. Sonnerup, "Magnetic-field re-connexion in a highly conducting incompressible fluid," *Journal of Plasma Physics, 4* (1970), 161.

88. T. Yeh and W. I. Axford, "On the re-connexion of magnetic field lines in conducting fluids," *Journal of Plasma Physics, 4* (1970), 207.

89. J. A. Van Allen and N. F. Ness, "Particle Shadowing by the Moon," *Journal of Geophysical Research, 74* (1969), 71.

90. K. A. Anderson, "Entry of Solar Cosmic Rays into the Earth's Magnetosphere," in *Particles and Fields in the Magnetosphere; Summer Advanced Study Institute, Symposium, University of California, Santa Barbara, California, August 4-15, 1969, Proceedings*, B. M. McCormac, ed., D. Reidel Publishing Co., Dordrecht, 1970, p. 3ff.

91. M. Siebert, "Magnetic Activity Differences between the Two Hemispheres following the Sector Structure of the Interplane-

tary Magnetic Field," *Journal of Geophysical Research, 73* (1968), 3049.

92. J. M. Wilcox, "Asymmetry in Geomagnetic Response to the Polarity of the Interplanetary Magnetic Field," *Journal of Geophysical Research, 73* (1968), 6835.

93. J. K. Hargreaves, "Conjugate and Closely-spaced Observations of Auroral Radio Absorption, III," *Planetary and Space Science, 17* (1969), 1919.

94. D. H. Fairfield, private communication, 1971.

95. R. Gall and A.Orozco, "On the Uneven Illumination of Polar Caps by Solar Cosmic Rays," *Transactions of the American Geophysical Union, 51* (1970), 800.

96. A. J. Dessler and R. D. Juday, "Configuration of Auroral Radiation in Space," *Planetary and Space Science, 13* (1965), 63.

97. F. C. Michel, "The Effect of Magnetospheric Tail on Cosmic Ray Cutoffs," *Planetary and Space Science, 13* (1965), 753.

98. F. C. Michel and A. J. Dessler, "The Physical Significance of Inhomogeneities in PCA Events," *Journal of Geophysical Research, 70* (1965), 4305.

99. A. J. Dessler, "Solar Wind Interactions," *(International Association of Geomagnetism and Aeronomy, Birkeland Symposium on Aurora and Magnetic Storms, Sandefjord, Norway, September 18-22, 1967), Annales de Géophysique, 24* (1968), 333.

100. A. J. Dessler, "Formation and Geometry of Geomagnetic Tail," in *Particles and Fields in the Magnetosphere; Summer Advanced Study Institute, Symposium, University of California, Santa Barbara, California, August 4-15, 1969, Proceedings*, B. M. McCormac, ed., D. Reidel Publishing Co., Dordrecht, 1970, p. 18ff.

101. L. C. Evans, "The Cross-sectional Shape of the Distant Geomagnetic Tail," Space Radiation Laboratory Internal Report No. 26, August, 1971.

102. J. W. Dungey, "The Structure of the Exosphere, or Adventures in Velocity Space," in *Geophysics, the Earth's Environment*, C. DeWitt, J. Hieblot, and A. Lebeau, eds., Gordon and Breach, New York, 1963, p. 504ff.

103. R. H. Levy, H. E. Petschek, and G. L. Siscoe, "Aerodynamic Aspects of the Magnetospheric Flow," *American Institute of Aernautics and Astronautics, 2* (1964), 2065.

104. W. J. Axford, H. E. Petschek, and G. L. Siscoe, "The Tail of the Magnetosphere," *Journal of Geophysical Research, 70* (1965), 1231.

105. J. W. Dungey, "The Length of the Magnetospheric Tail," *Journal of Geophysical Research, 70* (1965), 1753.

106. J. W. Dungey, "The Theory of the Quiet Magnetosphere," in *Solar-Terrestrial Physics*, J. N. King and W. S. Newman, eds., Academic Press, London, 1967, p. 91ff.

107. J. W. Dungey, "The Reconnection Model of the Magnetosphere," in *Earth's Particles and Fields; Proceedings of the NATO Advanced Study Institute, Freising, West Germany, July 31-August 11, 1967*, B. M. McCormac, ed., Reinhold Book Corp., New York, 1968, p. 385ff.

108. P. D. Hudson and H. R. Anderson, "Non-uniformity of Solar Protons over the Polar Caps on March 24, 1966," *Journal of Geophysical Research, 74* (1969), 2881.

109. L. A. Frank, "Plasma in the Earth's Polar Magnetosphere," to be published.

110. L. A. Frank and D. A. Gurnett, "On the Distribution of Plasmas and Electric Fields over the Auroral Zones and the Polar Caps," to be published.

111. J. R. Spreiter, A. L. Summers, and A. Y. Alksne, "Hydromagnetic Flow around the Magnetosphere," *Planetary and Space Science, 14* (1966), 223.

112. J. R. Spreiter and A. L. Summers, "On Conditions near the Neutral Points on the Magnetosphere Boundary," *Planetary and Space Science, 15* (1967), 787.

113. A. Y. Alksne, "Steady-state Magnetic Field in the Transition Region," *Planetary and Space Science, 15* (1967), 239.

114. H. E. Salzer, "Formulas for Calculating the Error Function of a Complex Variable," *Mathematical Tables and Aids to Computation, 5* (1951), 67 in W. Gautschi, "Error Function and Fresnel

Integrals," in *Handbook of Mathematical Functions with Formulas, Graphs, and Mathematical Tables*, M. Abramowitz and I. A. Stegun, eds., National Bureau of Standards, United States Department of Commerce, Washington D. C., 1964, p. 295ff.